Clinical Neurophysiology 162 (2024) 9–27

Contents lists available at ScienceDirect

Clinical Neurophysiology

journal homepage: www.elsevier.com/locate/clinph

Cortical and white matter substrates supporting visuospatial working memory

Riyo Ueda [a,b,1], Kazuki Sakakura [a,c,d,1], Takumi Mitsuhashi [a,e], Masaki Sonoda [a,f], Ethan Firestone [g], Naoto Kuroda [a,h], Yu Kitazawa [a,i], Hiroshi Uda [a,j], Aimee F. Luat [a,k,l], Elizabeth L. Johnson [m], Noa Ofen [n,o], Eishi Asano [a,k,p,*]

[a] Department of Pediatrics, Children's Hospital of Michigan, Detroit Medical Center, Wayne State University, Detroit, Michigan 48201, USA
[b] National Center Hospital, National Center of Neurology and Psychiatry, Tokyo 1878551, Japan
[c] Department of Neurosurgery, Rush University Medical Center, Chicago, Illinois 60612, USA
[d] Department of Neurosurgery, University of Tsukuba, Tsukuba 3058575, Japan
[e] Department of Neurosurgery, Juntendo University, School of Medicine, Tokyo 1138421, Japan
[f] Department of Neurosurgery, Yokohama City University, Yokohama 2360004, Japan
[g] Department of Physiology, Wayne State University, Detroit, Michigan 48202, USA
[h] Department of Epileptology, Tohoku University Graduate School of Medicine, Sendai 9808575, Japan
[i] Department of Neurology and Stroke Medicine, Yokohama City University, Yokohama 2360004, Japan
[j] Department of Neurosurgery, Osaka Metropolitan University Graduate School of Medicine, Osaka 5458585, Japan
[k] Department of Neurology, Children's Hospital of Michigan, Detroit Medical Center, Wayne State University, Detroit, Michigan 48201, USA
[l] Department of Pediatrics, Central Michigan University, Mt. Pleasant, Michigan 48858, USA
[m] Departments of Medical Social Sciences, Pediatrics, and Psychology, Northwestern University, Chicago, Illinois 60611, USA
[n] Life-Span Cognitive Neuroscience Program, Institute of Gerontology and Merrill Palmer Skillman Institute, Wayne State University, Detroit, Michigan 48202, USA
[o] Department of Psychology, Wayne State University, Detroit, Michigan 48202, USA
[p] Translational Neuroscience Program, Wayne State University, Detroit, Michigan 48201, USA

HIGHLIGHTS

- High memory loads enhance functional connectivity via occipital longitudinal tracts.
- High memory loads reduce functional connectivity via arcuate, uncinate, and superior longitudinal fasciculi.
- Task familiarity increases high-gamma amplitude in the inferior frontal gyrus, and its amplitude predicts successful recall.

ARTICLE INFO

Article history:
Accepted 11 March 2024
Available online 18 March 2024

Keywords:
Physiological high-frequency oscillations (HFOs)
Broadband high-frequency activity
Intracranial EEG recording
Functional brain mapping
Pediatric epilepsy surgery

ABSTRACT

Objective: In tasks involving new visuospatial information, we rely on working memory, supported by a distributed brain network. We investigated the dynamic interplay between brain regions, including cortical and white matter structures, to understand how neural interactions change with different memory loads and trials, and their subsequent impact on working memory performance.
Methods: Patients undertook a task of immediate spatial recall during intracranial EEG monitoring. We charted the dynamics of cortical high-gamma activity and associated functional connectivity modulations in white matter tracts.
Results: Elevated memory loads were linked to enhanced functional connectivity via occipital longitudinal tracts, yet decreased through arcuate, uncinate, and superior-longitudinal fasciculi. As task familiarity grew, there was increased high-gamma activity in the posterior inferior-frontal gyrus (pIFG) and diminished functional connectivity across a network encompassing frontal, parietal, and temporal lobes. Early

Abbreviations: AUC, area under the curve; CI, confidence interval; DWI, diffusion-weighted imaging; EEG, electroencephalography; FDR, false discovery rate; fMRI, functional magnetic resonance imaging; iEEG, intracranial electroencephalography; pIFG, posterior inferior-frontal gyrus; ITG, inferior-temporal gyrus; MEG, magnetoencephalography; aMFG, anterior middle-frontal gyrus; pMFG, posterior middle-frontal gyrus; MRI, magnetic resonance imaging; MTG, middle-temporal gyrus; ROIs, regions of interest; SFG, superior-frontal gyrus; STG, superior-temporal gyrus.

* Corresponding author at: Division of Pediatric Neurology, Children's Hospital of Michigan, Wayne State University 3901 Beaubien St., Detroit, MI 48201, USA.
E-mail addresses: hj9794@wayne.edu (R. Ueda), Kazuki_Sakakura@rush.edu (K. Sakakura), tmituha@juntendo.ac.jp (T. Mitsuhashi), sonoda.mas.pu@yokohama-cu.ac.jp (M. Sonoda), efirest@med.wayne.edu (E. Firestone), naoto.kuroda@wayne.edu (N. Kuroda), yu_kitazawa@wayne.edu (Y. Kitazawa), hm9480@wayne.edu (H. Uda), aluat@dmc.org (A.F. Luat), eljohnson@northwestern.edu (E.L. Johnson), noa.ofen@wayne.edu (N. Ofen), easano@med.wayne.edu (E. Asano).
[1] Equal contribution.

https://doi.org/10.1016/j.clinph.2024.03.008

pIFG high-gamma activity was predictive of successful recall. Including this metric in a logistic regression model yielded an accuracy of 0.76.
Conclusions: Optimizing visuospatial working memory through practice is tied to early pIFG activation and decreased dependence on irrelevant neural pathways.
Significance: This study expands our knowledge of human adaptation for visuospatial working memory, showing the spatiotemporal dynamics of cortical network modulations through white matter tracts.

1. Introduction

Visuospatial working memory involves encoding, temporary maintenance, and retrieval of visual and spatial information (Baddeley, 1992; Ma et al., 2014) and is essential for everyday cognitive function. Increased familiarity with a given task through practice improves working memory performance (Crone et al. 2006; Miotto et al., 2006; Schneiders et al., 2011; Kundu et al., 2013; Constantinidis and Klingberg, 2016; Thompson et al., 2016; Wang et al., 2019). The utilization of visuospatial working memory involves a distributed network of brain regions that work together to encode, maintain, and retrieve information. This network includes the lower- and higher-order visual areas, medial-temporal regions, dorsolateral prefrontal cortices, and the posterior inferior-frontal gyrus (pIFG) (Smith and Jonides, 1999; Constantinidis and Klingberg, 2016; Wu and Buckley, 2022). Converging evidence for the involvement of these brain regions in visuospatial working memory has been provided by functional MRI (fMRI) (LaBar et al., 1999; Pochon et al., 2001; Kwon et al., 2002; Krasnow et al., 2003; Croizé et al., 2004; Suchan et al., 2006; Ganis et al., 2007; Schmidt et al., 2007; Srimal and Curtis, 2008; Edin et al., 2009; Michels et al., 2010; Christophel and Haynes, 2014; Vetter et al., 2014; Zumer et al., 2014; Darki and Klingberg, 2015; Schmidt and Blankenburg, 2018; Yaple et al., 2019; Henderson et al., 2022), electrophysiology (Croizé et al., 2004; Vogel and Machizawa, 2004; Sauseng et al., 2005; Agam and Sekuler, 2007; Axmacher et al., 2008; Michels et al., 2010; Reinhart et al., 2012; Roux et al., 2012; Lozano-Soldevilla et al., 2014; Zumer et al., 2014; Johnson et al., 2018a; Sato et al., 2018; Reinhart and Nguyen, 2019; Goddard et al., 2022; Pavlov and Kotchoubey, 2022), and lesion-to-deficit studies (Ferreira et al., 1998; Hillary et al., 2006; Olson et al., 2006; Chase et al., 2008; Kas et al., 2011; Jeneson et al., 2012; Bowren et al., 2020). The initial processing of visuospatial information is carried out by lower- and higher-order visual areas in the occipital and temporal lobes within 200 ms after stimulus onset (Vogel and Machizawa, 2004; Agam and Sekuler, 2007; Reinhart and Nguyen, 2019; Peylo et al., 2022). Investigators have further highlighted the causal role of the medial temporal lobe in visuospatial working memory encoding and maintenance, in addition to the formation and retrieval of long-term memory (Olson et al., 2006; Axmacher et al., 2008; Jeneson et al., 2012; Suthana et al., 2015; Wu and Buckley, 2022). Meanwhile, the dorsolateral prefrontal cortices and pIFG are suggested to play a critical role in the maintenance and manipulation of mental representations of visuospatial information (Ferreira et al., 1998; Hillary et al., 2006, Chase et al., 2008; Johnson et al., 2017; Davoudi et al., 2021; Parto Dezfouli et al., 2021). fMRI studies have clarified the spatial extent of functional connectivity modulations during visuospatial working memory tasks, as defined by time-specific co-activation (or co-deactivation) in two distinct cortical regions, and the network showing such task-related enhancement of functional connectivity involved extensive regions, including the prefrontal and visual cortices of each hemisphere (Toepper et al., 2014; Elton and Gao, 2015; Shine et al., 2015; Galeano Weber et al., 2017; O'Connell and Basak, 2018; Di and Biswal, 2019; Finc et al., 2020; Lugtmeijer et al., 2023). However, the temporal dynamics of functionally-connected neural networks underlying visuospatial working memory, along with their supporting white matter tracts, are poorly understood. It is also unclear how these dynamics adapt as humans become familiarized with a task across successive trials and how these changes contribute to improvement of working memory performance.

This study aimed to investigate the dynamic pattern of neuronal activity conveyed through defined white matter tracts that support visuospatial working memory processes. To achieve this, we utilized a 'dynamic tractography' technique that incorporates intracranial EEG (iEEG) recording and diffusion-weighted imaging (DWI) tractography (Kitazawa et al., 2023; Ono et al., 2023). As detailed in the methods section below, for example, we defined functional connectivity modulation in relation to memory load as the simultaneous presence of memory load effects on neural activity within two brain regions and the existence of direct DWI streamlines connecting them. To quantify memory load- and task familiarity-dependent effects on neural activity, we measured event-related high-gamma amplitude at 70–110 Hz, a surrogate marker of neural activation with excellent signal fidelity and temporal resolution (Crone et al., 2006; Nir et al., 2007; Ball et al., 2009; Burke et al., 2014; Buzsáki and Schomburg, 2015; Rich et al., 2017; Sonoda et al., 2022). Event-related high-gamma augmentation is tightly correlated with increased firing rate on single neuron recordings (Mukamel et al., 2005; Ray et al., 2008; Rich and Wallis, 2017; Leszczyński et al., 2020), increased hemodynamic activation on fMRI (Nir et al., 2007; Harvey et al., 2013; Kunii et al., 2013; Hill et al., 2021), and increased glucose metabolism on positron emission tomography (PET) (Nishida et al., 2008), and correlates with behavioral changes induced by direct cortical stimulation (Arya et al., 2018). We previously found that event-related high-gamma amplitude modulation was a better predictor of cognitive outcomes after cortical resection than event-related amplitude modulation of low-frequency bands (Sonoda et al., 2022). In the present study, we created animations illustrating when and where cortical high-gamma activity and functional connectivity through white matter tracts were modulated under varying levels of memory load and task familiarity. We tested the following hypotheses. First, we expected that brain regions supporting memory encoding and maintenance would exhibit high-gamma amplitude enhancement as *memory load* increased: specifically the visual cortex, medial temporal region, dorsolateral prefrontal cortices, and pIFG (Olson et al., 2006; Agam and Sekuler, 2007; Jeneson et al., 2012; Reinhart and Nguyen, 2019; Peylo et al., 2022; Wu and Buckley, 2022). Second, we predicted that specific brain regions, such as the dorsolateral prefrontal cortices or pIFG, would exhibit high-gamma enhancement as *task familiarity* increased from trial to trial (Ferreira et al., 1998; Hillary et al., 2006; Chase et al., 2008). We conducted a trial-by-trial analysis and examined whether the high-gamma amplitudes in the regions showing task familiarity-dependent enhancement were predictive of successful recall.

Why is there a need to employ intracranial EEG for evaluating the neural dynamics during visuospatial working memory tasks? Artifacts from the temporal and ocular muscles pose challenges to the quantitative measurement of event-related high-gamma activity via scalp EEG and magnetoencephalography (MEG). As such, many of the prior non-invasive studies on visuospatial working memory have largely reported on modulations of low-frequency band cortical signals instead. For example, noninvasive electrophysiology studies report augmentation of alpha and beta amplitudes during working memory tasks (Sauseng et al., 2005; Mazaheri and Jensen, 2008; van Dijk et al., 2010; Reinhart et al., 2012), while others report alpha and beta attenuation (Proskovec et al., 2018). It has been hypothesized that augmentation of event-related alpha/beta amplitudes during working memory tasks is indicative of disengagement of underlying cortical modules (Hanslmayr et al., 2016; Johnson et al., 2020; Yin et al., 2020). A tight inverse correlation has been reported between high-gamma and low-frequency band amplitudes in the primary sensory and motor cortices during spontaneous body movements (Crone et al., 2006; Ono et al., 2023). To enhance our understanding of working memory task-related modulations of low-frequency band activity, we explored the correlation between task-related amplitude modulations of high-gamma and low-frequency bands in each region of interest (ROI). We examined the possibility of an inverse relationship, in which the attenuation of high-gamma amplitudes would be associated with the augmentation of low-frequency band amplitudes at a given moment, and *vice versa*. We expected that the current study might offer insights into the potential mechanisms underlying modulations of low-frequency band activities during working memory tasks.

2. Methods

2.1. Participants

The present study included 10 participants (Table 1) who met the following eligibility criteria. The inclusion criteria were: (i) patients with focal epilepsy who underwent extraoperative iEEG recording as part of the clinical management of drug-resistant seizures at Children's Hospital of Michigan between September 2017 and September 2021; (ii) able to complete five sessions of *Memory Matrix* - a visuospatial working memory game on the Lumosity platform (https://www.lumosity.com/; Lumos Labs, Inc, San Francisco, CA) - during interictal iEEG recording. Participants were excluded if they had: (i) massive brain malformations that deformed the central, lateral, or calcarine sulcus (Kitazawa et al., 2023); (ii) a history of previous resective epilepsy surgery; (iii) hemiparesis; (iv) visual field deficit on confrontation; or (v) hearing deficit.

All 10 participants were right-handed, and none exhibited a congenital, left-hemispheric neocortical MRI lesion associated with left-handedness. Therefore, it was suggested that all patients had essential language areas located in the left hemisphere (Rasmussen and Milner, 1977; Akanuma et al., 2003; Möddel et al., 2009). We had a comprehensive discussion on the justification and reliability of estimating the language-dominant hemisphere through anatomical imaging and handedness (Sonoda et al., 2022). Indeed, electrical stimulation mapping identified left-hemispheric language sites in all six patients who underwent intracranial electrode sampling mainly from the left hemisphere (i.e., patients 1, 2, 3, 5, 6 and 10). No such sites were detected in the right hemisphere of any patient.

2.2. Intracranial EEG and MRI data acquisition

The data acquisition framework for iEEG and MRI data was the same as previously reported (Nakai et al., 2017; Johnson et al., 2018b; 2022; Yin et al., 2020; Mitsuhashi et al., 2022). Platinum disk electrodes with a 10 mm center-to-center distance were surgically placed on the pial surface of the brain (Fig. 1). The number and configuration of intracranial electrodes were based purely on clinical needs to localize the boundary between the epileptogenic zone and eloquent areas, and no extra electrodes were implanted for research purposes. Bedside iEEG recording in the Epilepsy Monitoring Unit was performed using a Nihon Kohden Neurofax 1100A Digital System (Nihon Kohden America Inc, Foothill Ranch, CA, USA) with a sampling rate of 1000 Hz and an amplifier bandpass filter of 0.016–300 Hz. The exact timing of stimulus onset and offset, as well as participants' tap responses, were integrated into the iEEG acquisition system via the DC input (Mitsuhashi et al., 2022). A total of 876 electrode sites were utilized for subsequent iEEG analysis, after excluding those located in the seizure onset zone (Asano et al., 2009), spiking zone (Kural et al., 2020), or structural lesions, along with those affected by artifacts.

Before intracranial electrode placement, we acquired 3-tesla MRI scans, which included T1-weighted spoiled gradient-recalled echo and fluid-attenuated inversion recovery sequences (Nakai et al., 2017). We used FieldTrip (https://www.fieldtriptoolbox.org) to create a 3D MRI surface image, where electrode locations were defined directly on the brain surface using post-implant CT images (Stolk et al., 2018). We next used FreeSurfer (https://surfer.nmr.mgh.harvard.edu) to normalize each electrode site to an MNI-standard brain coordinate for group-level visualization and analysis. We then divided the cerebral cortex of each hemisphere into 21 ROIs based on the Desikan parcellation (Desikan et al., 2006) and included 16 ROIs that contained at least 20 electrode sites in our group-level statistical analyses (Fig. 1).

2.3. Visuospatial working memory task

Patients completed the *Memory Matrix* in a quiet room, during their interictal state and at least two hours apart from habitual sei-

Table 1
Patient demographics. CLB: Clobazam. LAC: Lacosamide. LEV: Levetiracetam. LTG: Lamotrigine. OXC: Oxcarbazepine. TPM: Topiramate. VPA: Valproate. ZNS: Zonisamide, F: Frontal. O: Occipital. P: Parietal. T: Temporal. NA: Not available because seizure events did not occur during the iEEG recording.

Patient number	Age (years)	Sex	Sampled hemisphere	Number of analyzed electrodes	Antiepileptic drugs	Age of epilepsyonset (years)	Seizure onset zone	MRI finding
1	17	Male	Left	86	OXC, LEV	15	T	Nonlesional
2	11	Male	Left	74	OXC	6	T	Tumor
3	16	Male	Left	89	LEV	9	T	Tumor
4	20	Male	Right	105	VPA, OXC	6	F	Nonlesional
5	13	Male	Left	64	OXC, CLB, LAC	8	T	Heterotopia
6	9	Male	Left	64	OXC	9	T	Tumor
7	16	Female	Right	114	CLB, TPM	12	NA	Nonlesional
8	14	Female	Right	79	LAC, LTG	5	Insula	Tumor
9	15	Female	Right	106	LTG, ZNS	6	P	Nonlesional
10	19	Female	Left & Right	95	OXC	4	F	Nonlesional

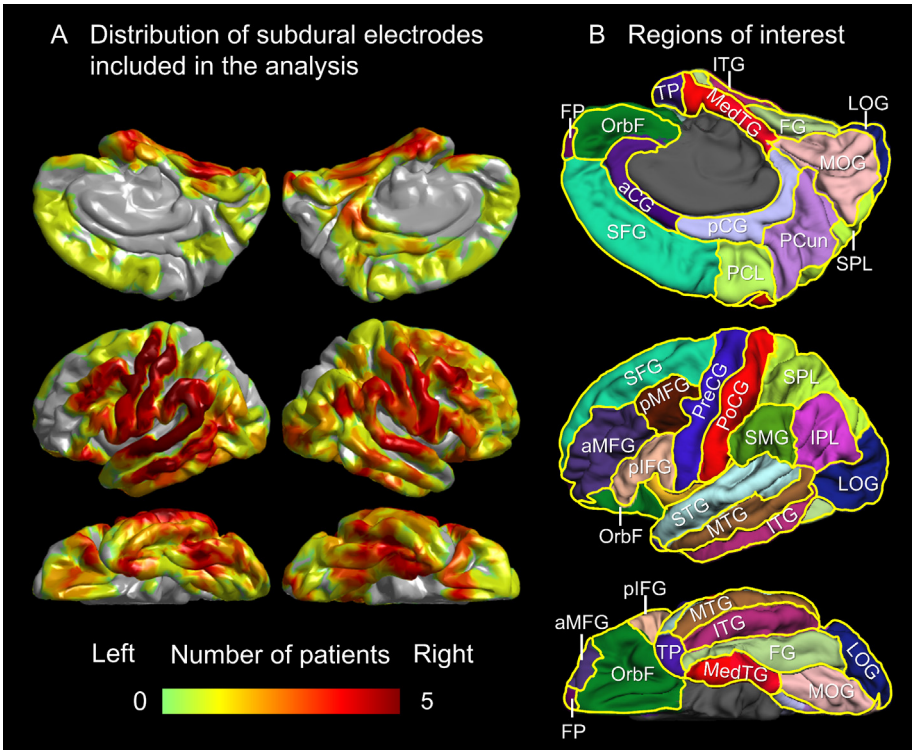

Fig. 1. Distribution of subdural electrode sites across regions of interest (ROIs). (A)The pooled distribution of electrode sites from 10 patients. (B) ROI locations. PreCG: precentral gyrus. PoCG: postcentral gyrus. STG: superior-temporal gyrus. aMFG and pMFG: anterior and posterior middle-frontal gyri. SMG: supramarginal gyrus. SFG: superior-frontal gyrus. FG: fusiform gyrus. pIFG: posterior inferior-frontal gyrus (summation of pars opercularis and pars triangularis). MedTG: medial temporal gyrus (summation of entorhinal and parahippocampal gyri). MTG: middle-temporal gyrus. LOG: lateral occipital gyrus. IPL: inferior parietal lobule. ITG: inferior-temporal gyrus. OrbF: orbitofrontal gyrus (summation of pars orbitalis and medial and lateral orbitofrontal gyri). MOG: medial occipital gyrus (summation of cuneus and lingual gyri). SPL: superior parietal lobule. A total of 16 regions of interest mentioned above were included in the group-level ROI analysis as they contained at least 20 electrode sites. In turn, the ROI analysis excluded the following regions that were sampled by fewer than 20 electrode sites. aCG: anterior cingulate gyrus. PCun: precuneus gyrus. pCG: posterior cingulate gyrus. PCL: paracentral lobule. FP: frontal pole. Supplementary Table 1 presents the precise count of electrode sites in the respective ROIs.

zure events (Fig. 2; **Supplementary Video 1**). None of the patients had played this working memory game before, and all patients were given a brief tutorial to understand the rules prior to the first session. Patients were comfortably positioned on bed, and used an iPad (screen display width: 14.7 cm; length: 19.6 cm; Apple Inc., Cupertino, CA) to play five consecutive sessions, each comprising 12 trials. During a given trial, a tile grid with *n* blue-painted tiles was displayed on the iPad screen for two seconds. Patients were required to remember the locations of the blue tiles, and following their disappearance, tap on the locations where they were previously presented, using their right finger. After the *n*-th tap response, the screen was refreshed, and another trial began. The game was designed such that the number of presented blue tiles was adjusted based on the accuracy of preceding trials. Memory load increased by one tile after a successful trial, and decreased by one tile after a failed trial. The first trial consisted of 3 blue tiles and maximum number of tiles in a single trial was 13 in the present study. A trial was considered a 'success' when all tile locations were accurately tapped and as 'failure' otherwise. The response time for a given trial was defined as the period between stimulus offset and onset of the initial tap response.

2.4. Time-frequency analysis of high-gamma activity in iEEG

We employed time–frequency iEEG analysis on common average reference, as previously reported (Nakai et al., 2019; Mitsuhashi et al., 2022; Kitazawa et al., 2023; Ono et al., 2023). The complex demodulation method incorporated in the BESA EEG Analysis Package (BESA GmbH, Gräfelfing, Germany; Hoechstetter et al., 2004; Papp and Ktonas, 1977) transformed iEEG signals into 10-ms/5-Hz time–frequency bins for assessment of high-gamma amplitude$_{70\text{-}110\ Hz}$ during the following periods: [1] the 3,000-ms time window between the stimulus onset and 1,000 ms after the stimulus offset; and [2] the 2,000-ms time window 1500-ms before and 500-ms after the initial tap response. The complex modulation was done by multiplying the time-domain iEEG signal with a complex exponential, followed by a band-pass filter. Because it employed a Gaussian-shaped low-pass finite impulse response filter, this complex demodulation method is equivalent to a Gabor transformation. The time–frequency resolution for high-gamma measurement was ± 15.8 ms and ± 7.1 Hz (defined as the 50% power drop of the finite impulse response filter).

To visualize the spatiotemporal dynamics of high-gamma modulations, we calculated the percent change in high-gamma amplitude for each electrode site (where amplitude is a measure proportional to the square root of power), in comparison to a baseline mean. To establish baseline, we selected 60 non-overlapping 2,000-ms time windows during periods of spontaneous, resting, eye-open wakefulness immediately preceding the game sessions. We then visualized the percentage change in high-gamma amplitude on a FreeSurfer standard pial surface image, applying interpolation within 10 mm from the electrode center (Sakakura et al. 2022; **Supplementary Video 2**).

To assess the correlation between task-related amplitude modulations of high-gamma and other frequency bands, at a given moment, we analyzed the iEEG signals using the non-overlapping time–frequency bins designed to provide optimal frequency resolution for lower-frequency bands. To quantify the amplitude of delta (2–4 Hz) activity, the complex demodulation method transformed iEEG signals into 50-ms/1-Hz time–frequency bins,

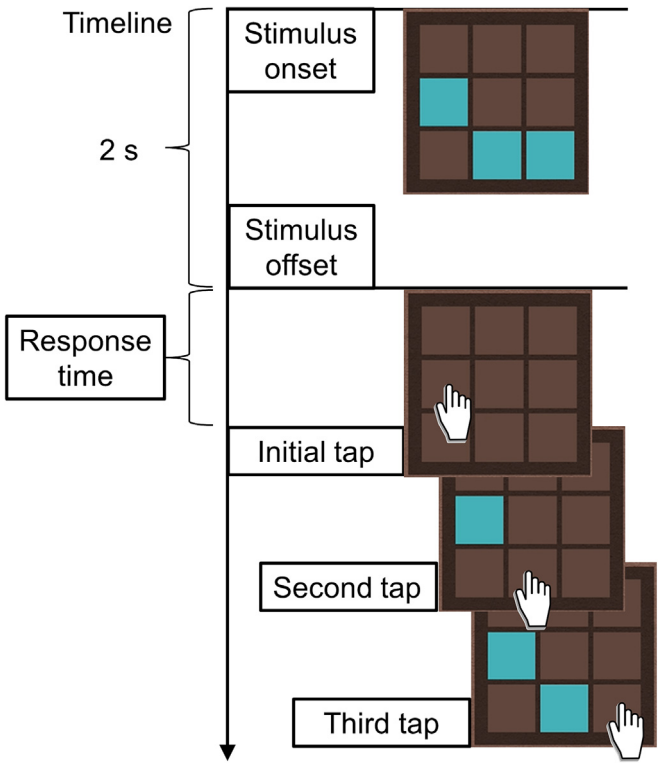

Fig. 2. ***Memory Matrix*: a visuospatial working memory game.** Each trial involved remembering the locations of blue-painted tiles visible for two seconds. After the blue tiles disappeared, patients tapped on the remembered locations. A feedback sign and sound were given immediately following each tap to indicate if the response was correct. After the *n*-th tap (in this case, *n* = 3), the screen was refreshed and the next trial began. The stimulus period was defined as the two-second period between stimulus onset and offset, while the response period was defined as the time between stimulus offset and the *n*-th tap. **Supplementary Video 1** demonstrates how to play this iPad-based memory game. As the number of blue-painted tiles increased, the matrix size (row × column) increased as follows: 3 tiles: 3 × 3; 4 tiles: 3 × 4; 5 tiles: 4 × 4; 6 tiles: 4 × 5; 7 tiles: 5 × 5; 8–9 tiles: 5 × 6; 10–13 tiles: 6 × 6.

providing a time–frequency resolution of ± 79 ms and ± 1.4 Hz for this band. To quantify the amplitude of theta (4–8 Hz), alpha (8–12 Hz), sigma (12–16 Hz), beta (16–30 Hz), low-gamma (30–50 Hz), high-gamma (70–110 Hz), and very high-gamma (130–150 Hz) frequencies, we used 25-ms/2-Hz time–frequency bins. This provided a time–frequency resolution of ± 39.4 ms and ± 2.8 Hz for these bands.

2.5. Statistical assessment of factors associated with task-related high-gamma modulations

We employed a mixed model analysis to investigate whether increased memory loads or task familiarity altered the spatiotemporal characteristics of high-gamma amplitude modulations during a visuospatial working memory task. We tested the prediction that high-gamma amplitude increases as a function of memory load in region including the visual cortex, medial temporal region, dorsolateral prefrontal cortices, and pIFG. In turn. Furthermore, we tested the prediction that task familiarity would be associated with high-gamma increases in dorsolateral prefrontal cortices and pIFG.

The dependent variable was the high-gamma amplitude at each electrode site (% change compared to the baseline mean), at a specific ROI, during a given 250-ms window slide, moving every 50 ms through the 2,500-ms analysis period between stimulus onset and 500 ms after stimulus offset, in each trial. The fixed effect predictor variables included [a] 'number of blue tiles' (ranging from 3 to 13) treated to represent the working memory load in a given trial, and [b] 'trial number' (ranging from 1 to 60), representing the degree of task familiarity. We controlled potential confounding effects on high-gamma amplitude measures by incorporating the following fixed effect variables: [c] 'patient age' (in years), [d] 'sampled hemisphere' (with a value of 1 indicating the left hemisphere), [e] 'individual recall performance' (defined as the median number of blue tiles among successful trials; ranging from 6 to 9), and [f] 'immediately prior failure' (with a value of 1 indicating a failure in the immediately preceding trial). The rationale for incorporating 'patient age' into the mixed model analysis was to account for the anticipated development and improvement of visuospatial working memory skills during childhood and adolescence, as noted by prior research (Vuontela et al., 2003). Given our small sample size of ten, this analysis was not intended to definitively identify a statistically significant developmental variability (Johnson et al., 2022; Johnson and Knight, 2023). The effect of 'sampled hemisphere' was considered because visuospatial processing tends to be right-hemispheric dominant (Pisella et al., 2011; Mankin et al., 2021), and all participants were right-handed and responded with their right fingers, in the present study. We also considered the effect of 'individual recall performance' since patients with higher working memory performance would require a larger number of blue tiles to pose a measurable increase in memory load. In addition, we considered the impact of a failure in the immediately preceding trial because this adaptive working memory task was designed to pose a memory load of '*m*' immediately following a successful trial with a load of '*m*-1′ or immediately following a failed trial with a load of '*m* + 1′. We likewise considered the possibility that patients may become more cautious in the trial immediately after a failure (Mitsuhashi et al., 2022). Patient and intercept were treated as random factor variables. We employed a false discovery rate (FDR) correction for repeated modeling of 16 ROIs across 46 sliding time windows, and the threshold for statistical significance was set at a two-sided FDR-corrected p-value less than 0.05.

2.6. Definition and visualization of memory load-related and task familiarity-related modulations of functional connectivity

To visualize the spatiotemporal characteristics of memory load-related functional connectivity modulations via white matter tracts, we created a dynamic tractography animations using a method similar to those reported previously (**Supplementary Video 3**; Kitazawa et al., 2023; Ono et al., 2023). The mixed model analysis, performed in the previous section, determined the time windows in which the memory load showed a significant positive (or negative) effect on high-gamma amplitude, at given pairs of cortical ROIs (Fig. 1**B**). We thereby declared the 'functional connectivity' between white matter-connected ROIs to be enhanced (or diminished), as a function of the memory load if: [i] both ROIs showed significant and simultaneous memory load effects on the mixed model analysis and [ii] they were connected by direct DWI streamlines. Thereby, we defined the onset latency of high-gamma functional connectivity based on the timing of significant co-modulations via white matter tracts.

To delineate anatomical white matter streamlines, we utilized open-source DWI data collected from 1,065 healthy participants as part of the Human Connectome Project (Yeh et al., 2018; https://brain.labsolver.org/diffusion-mri-templates/hcp-842-hcp-1021); a method previously reported in our work (Mitsuhashi et al., 2021; Sonoda et al., 2021; Mitsuhashi et al., 2022; Kitazawa et al., 2023; Ono et al., 2023; Sakakura et al., 2023). To identify white matter tracts underlying functional connectivity modulations, we placed seeds at cortical ROIs revealing significant and simultaneous

positive (or negative) memory load effects on high-gamma amplitude, as determined by the mixed model analysis. The DSI Studio script (https://dsi-studio.labsolver.org/) visualized tractography streamlines directly connecting these cortical ROIs within the Montreal Neurological Institute standard space. The fiber tracking parameters used were a quantitative anisotropy threshold of 0.05, a maximum turning angle of 70° and a streamline length of 20 to 250 mm. We excluded streamlines involving the brainstem, basal ganglia, thalamus, or cerebrospinal fluid space from the tractography analysis. The resulting dynamic tractography videos - sliding every 50 ms during the 2,500-ms analysis period between stimulus onset and 500 ms after stimulus offset - visualized the spatiotemporal dynamics of white matter streamlines linking functionally connected sites with significant memory load effects on high-gamma amplitude (**Supplementary Video 3**). In the present study, we visualized memory load effects on high-gamma amplitudes in one hemisphere; using mixed model analysis, we clarified whether the sampled hemisphere had a significant effect on high-gamma amplitudes at given ROIs and time windows.

We likewise generated another dynamic tractography video animating the spatiotemporal characteristics of task familiarity-related functional connectivity modulations via white matter tracts (**Supplementary Video 4**). We considered the functional connectivity through given white matter tracts to be enhanced (or diminished), as a function of task familiarity, if a given ROI pair showed a significant and simultaneous effect of 'trial number' on high-gamma amplitude in the mixed model analysis and if they were connected by direct DWI streamlines.

2.7. Per-trial statistical assessment of the relationship between high-gamma modulations and response accuracy

Using a logistic mixed model analysis, we aimed to investigate whether high-gamma modulations, at a given ROI in a given trial, would be associated with improved recall performance. This analysis tested the hypothesis that enhanced high-gamma amplitudes at dorsolateral prefrontal or pIFG ROIs would be associated with improved response accuracy. The dependent variable was 'response accuracy' (with a value of 1 indicating the correct response) in a given trial. The fixed effect predictor variables included [a] 'number of blue tiles' (reflecting memory load) in a given trial, [b] 'trial number' (reflecting task familiarity), [c] 'patient age', [d] 'sampled hemisphere', [e] 'individual recall performance', [f] 'failure in an immediately prior trial', and [g] 'mean high-gamma' (percent change during a given non-overlapping 250-ms time window at the ROI). Patient and intercept were treated as random factor variables. We employed an FDR correction for repeated modeling for ROIs across the 2,500 ms analysis period between stimulus onset and 500 ms after stimulus offset, and the threshold for statistical significance was set at a two-sided FDR-corrected p-value less than 0.05.

2.8. Statistical assessment of the additive value of high-gamma amplitude in predicting upcoming responses

It is plausible to expect that trials with lower memory loads would be associated with a higher chance of successful recall. We assessed the extent to which addition of an early high-gamma measure during the stimulus period could enhance the accuracy of a prediction model that solely incorporates memory load. To do so, we employed a method analogous to those previously reported (Kuroda et al., 2021; Sonoda et al., 2022).

First, we utilized a machine learning-based analysis to explore which of the high-gamma measures among 16 ROIs and four 250-ms time windows during the first 1,000 ms period after stimulus onset served as the most effective classifier for predicting a patient's response. We employed the ensemble learning algorithm provided by the Statistics and Machine Learning Toolbox in MATLAB R2022b (https://www.mathworks.com/help/stats/ensemble-algorithms.html). We generated the bagged tree ensemble model based on 'number of blue tiles', 'trial number', 'patient age', 'individual recall performance', 'immediately prior failure', and 'mean high-gamma', in a given non-overlapping 250-ms time window at each of the 16 ROIs. Using the MATLAB 'predictorImportance' function (https://www.mathworks.com/help/stats/compactregressionensemble.predictorimportance.html; AlSkaif et al., 2020), we computed the relative importance of each variable in predicting a successful trial 100 times, and the one-sample t-test subsequently determined which variable had the highest mean relative importance in this machine learning-based classification of successful trials. It should be noted that, in the bagged tree ensemble model analysis, we utilized a five-fold cross-validation procedure whereby the 60-trial data was randomly partitioned into five sets. The algorithm was trained on four of these sets, representing 80% of the trials, while the remaining set (20% of the trials) was used for testing the model's performance. We hypothesized that high-gamma augmentation in the dorsolateral prefrontal cortex or pIFG would emerge as the most significant contributing factor in predicting the accuracy of forthcoming responses.

Next, we determined the utility of task-related high-gamma amplitude in predicting forthcoming response accuracy. To this end, we employed logistic regression analysis at each electrode site to quantify the impact of incorporating high-gamma amplitude on the model's accuracy in predicting a patient's upcoming response. We initially assessed the prediction accuracy of 'the base logistic regression model' solely incorporating the number of blue tiles (i.e., memory load in a given trial). We then assessed the prediction accuracy of 'the full logistic regression model', which also incorporated the mean high-gamma amplitude (% change) during a 250-ms time window at the specific ROI identified by the machine learning algorithm as the most important contributing variable. We assessed the prediction accuracy of each logistic regression model using area under the receiver operating characteristics curve. We employed a leave-one trial-out cross-validation procedure to reduce the risk of overfitting to the training data. We performed the statistical analyses using IBM SPSS Statistics 25 software (IBM Corp., Chicago, IL, USA). A two-sided p-value of < 0.05 was considered statistically significant.

2.9. Statistical assessment of the relationship between high-gamma and other frequency band amplitudes

In each ROI, we investigated whether the attenuation of high-gamma amplitudes was associated with an increase in low-frequency band amplitudes at any given moment, and *vice versa*. To this end, we computed the Spearman's rho at each electrode site, reflecting the correlation between the amplitudes of high-gamma and each of the lower frequency bands (i.e., theta, alpha, sigma, beta, low-gamma, and very high-gamma) across 120 non-overlapping time bins within a 3,000-ms period spanning from stimulus onset to 1,000 ms after stimulus offset. The Spearman's rho was likewise computed between high-gamma and delta amplitudes across 60 non-overlapping time bins within the same period. We then used studentized bootstrap statistics, with 1,000 resamples, to test if the mean Spearman's rho significantly differed from zero at each ROI. A negative Spearman's rho would imply an inverse correlation between high-gamma and given frequency band amplitudes, at a given ROI. A two-sided p-value of < 0.05 was considered statistically significant.

2.10. Ethics statement

The Institutional Review Board at Wayne State University approved this study. We obtained written informed consent from

patients 18 years or older or the legal guardians of patients younger than 18. We also obtained written assent from pediatric patients aged 13 years or older.

2.11. Data availability

The iEEG data is available at https://openneuro.org/ (https://doi.org/10.18112/openneuro.ds004770.v1.0.0).

2.12. Code availability

The analysis codes are available at https://github.com/kaz1126/MI_HFO.

3. Results

3.1. Behavioral observations

All patients confirmed that the session was their first time using the assigned memory task game. All patients completed 60 trials, and the individual recall performance (defined as the median number of blue tiles among all successful trials) ranged from 6 to 9. The maximum number of blue tiles (i.e., maximum memory load) in successful trials ranged from 8 to 12 across patients, while in failed trials it ranged from 9 to 13. The mean response time was 1,169 ms (range: 814 to 2,081 ms), and the mean correct response rate was 52.3% (range: 46.7% to 58.3%). Immediately after a successful trial, the mean response time was 1,234 ms (range across patients: 883 to 2,130 ms), and it was 1,229 ms (range: 789 to 2081 ms) immediately after a failed trial.

The behavioral data did not show evidence of excessive multicollinearity across 'memory load (i.e., tile number)', 'task familiarity (i.e., trial number)', and 'failed response in an immediately prior trial'. Regression analyses indicated that the average correlation coefficient across the 10 patients, with the standard deviation in parentheses, was 0.262 (0.205) between 'memory load' and 'task familiarity'; 0.103 (0.085) between 'memory load' and 'failed response in an immediately prior trial'; and 0.129 (0.063) between 'task familiarity' and 'failed response in an immediately prior trial'.

The mixed model analysis, incorporating 'memory load', 'task familiarity', 'patient age', 'individual recall performance' and 'failed response in an immediately prior trial' as fixed effect predictors while 'patient' and 'intercept' as random factors, demonstrated that increased memory load was associated with increased response times (t-value: 2.70; mixed model coefficient: 49 ms/tile; 95% confidence interval [95%CI]: 13 to 85; p-value: 0.007; degrees of freedom [DF]: 579.28). In addition, increased task familiarity was associated with reduced response times (t-value: −2.29; mixed model coefficient: −4 ms/trial; 95%CI: −7 to − 1; p-value: 0.022; DF: 577.10). Patients with greater individual recall performance also demonstrated reduced response times (t-value: −3.80; mixed model coefficient: −310 ms/tile; 95%CI: −500 to − 120; p-value: 0.006; DF: 7.56). Alternatively, the mixed model analysis failed to find a significant effect of 'patient age' (t-value: −1.45, mixed model coefficient: −38 ms; 95%CI: −99 to 24; p-value: 0.190; DF: 7.00) or 'failed response in an immediately prior trial' (t-value: −0.17; mixed model coefficient: −10 ms; 95%CI: −119 to 100; p-value: 0.862; DF: 577.2).

3.2. Memory load-dependent high-gamma amplitude modulations

Findings from the mixed model analysis are presented in Fig. 3 and described below. With increased memory load, there was a significant increase in high-gamma amplitude in several brain regions at different time points after stimulus onset. The medial occipital region showed a sustained memory load-dependent increase in high-gamma amplitude right after stimulus onset (maximum t-value: +3.36 at the 250-ms period between + 350 to + 600 ms post-stimulus onset; mixed model coefficient: +1.78%/tile; 95%CI: +0.74 to + 2.82; uncorrected p-value: 0.001; DF: 1701.98), followed by the medial temporal region (maximum t-value: +2.90 between + 550 to + 800 ms post-stimulus onset; mixed model coefficient: +1.75%/tile; 95%CI: +0.57 to + 2.94; uncorrected p-value: 0.004; DF: 1701.12), fusiform area (maximum t-value: +2.61 between + 550 to + 800 ms post-stimulus onset; mixed model coefficient: +1.03%/tile; 95%CI: +0.25 to + 1.80; uncorrected p-value: 0.009; DF: 3588.55), and lateral occipital regions (maximum t-value: +2.11 between + 550 to + 800 ms post-stimulus onset; mixed model coefficient: +1.05%/tile; 95%CI: +0.07 to + 2.03; uncorrected p-value: 0.035; DF: 2173.84).

In contrast, with increased memory load there was significant reduction of high-gamma amplitude in several brain regions including the superior-temporal gyrus (STG), precentral gyrus, anterior middle frontal gyrus (aMFG), posterior middle frontal gyrus (pMFG), orbitofrontal gyrus, pIFG, superior-frontal gyrus (SFG), and supramarginal gyrus (largest negative t-value noted at STG: −7.77 between + 100 to + 350 ms post-stimulus onset; mixed model coefficient: −1.98%/tile [95%CI: −2.47 to − 1.48]; uncorrected p-value: 9.96E-15; DF: 4708.37; Fig. 3).

3.3. Memory load-dependent functional connectivity modulations

As best demonstrated in the dynamic tractography video (Fig. 3**C; Supplementary Video 3**), with increased memory load, there was an increase in the functional connectivity through the medial occipital longitudinal tract (Beyh et al., 2022) connecting the medial occipital and medial temporal regions between 350 and 800 ms post-stimulus onset. Similar effects were observed for the inferior longitudinal and vertical occipital fasciculi connecting the medial occipital, lateral occipital, fusiform, and medial temporal regions between 550 and 950 ms post-stimulus onset. Similar effects were also observed for the inferior fronto-occipital fasciculus connecting the medial occipital and pIFG between − 100 and 200 ms post-stimulus offset. Mixed model analysis revealed that 49 time bins showed significant positive memory load effects on high-gamma amplitudes. Considering the presence of 120 distinct pairs of analysis ROIs in the present study, there was approximately 41.3%, 0.2%, and 0.001% chance probability of a pair of ROIs showing significant positive memory load effects simultaneously for at least one, two, or three consecutive time windows, respectively. Here, the chance probability of simultaneous occurrence of significant positive memory load effects at least at a pair of ROIs for consecutive x time windows was based on the following equation: $1 - (1 - ((49/736)^2)^x)^{120}$.

With increased memory load, there was a decrease in the functional connectivity in several white matter tracts including the arcuate, uncinate, and superior-longitudinal fasciculi connecting the temporal, frontal, and parietal lobes between the stimulus onset and 500 ms post-stimulus offset (Fig. 3**C; Supplementary Video 3**). Mixed model analysis revealed that 195 time windows (or 26.5%) showed significant negative memory load effects on high-gamma amplitudes. Thus, there was approximately 45.4%, 4.2%, and 0.3% chance probability of a pair of ROIs showing significant negative memory load effects simultaneously for at least two consecutive, three consecutive, and four consecutive time windows.

3.4. Task familiarity-dependent high-gamma amplitude modulations

The mixed model analysis showed that, with increased trial number, there was a significant increase in high-gamma amplitude in the pIFG between + 400 ms and + 900 ms post-stimulus onset (maximum t-value: +3.77 noted at a 250-ms period between + 800

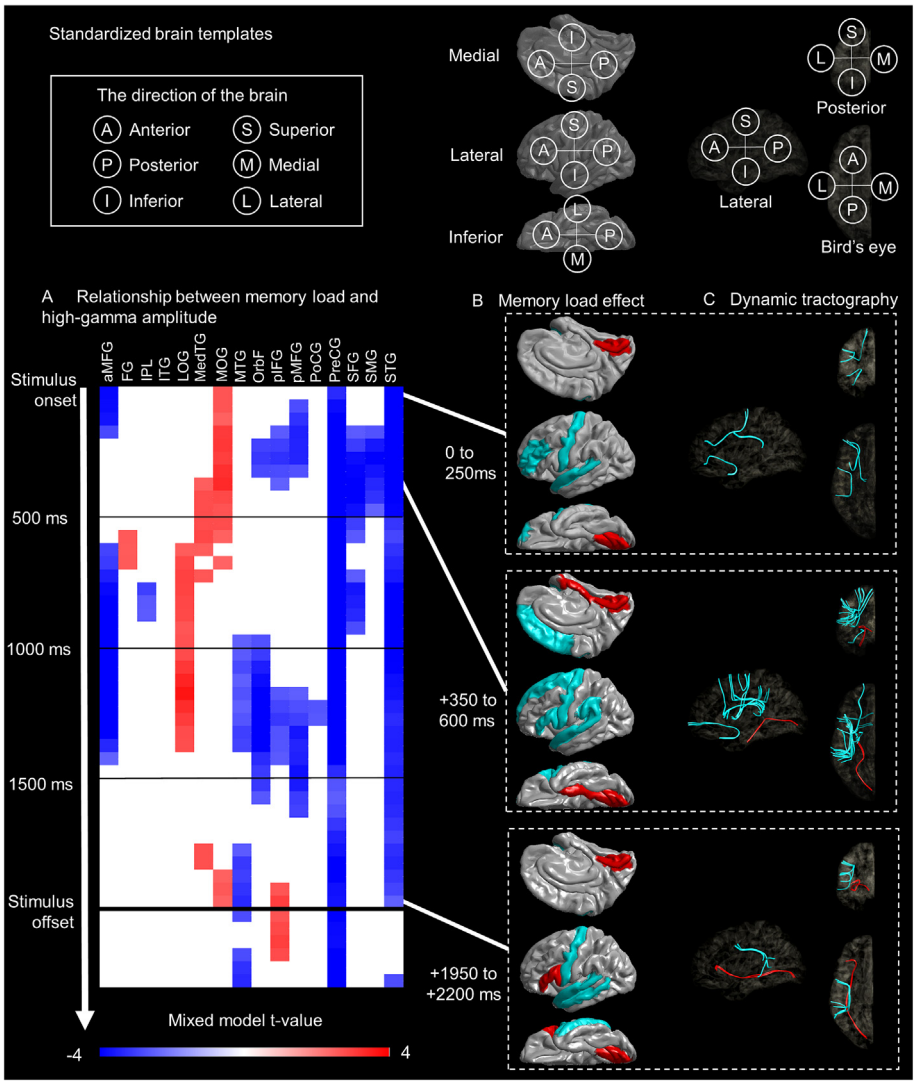

Fig. 3. Memory load-dependent high-gamma amplitude modulations and white matter substrates. (A) Spatiotemporal characteristics of the relationship between memory load and high-gamma amplitude. The red cells indicate mixed model t-values at regions of interest (ROIs) and corresponding 250-ms time windows (sliding every 50 ms) where increased memory loads were significantly associated with higher high-gamma amplitudes (i.e., FDR-corrected p-value < 0.05). The blue cells indicate spatiotemporal locations where increased memory loads were significantly associated with decreased high-gamma amplitudes. (B) Snapshots of memory load-dependent high-gamma modulations on the cortical surface. Color-coded ROIs indicate that increased memory loads were significantly associated with increased (red) or decreased (blue) high-gamma amplitudes. (C) Snapshots of white matter tracts underlying memory load-dependent functional connectivity modulations. Color-coded streamlines indicate functional connectivity enhancement (red) and diminution (blue) between ROIs. 0 ms: a 250-ms time window immediately after stimulus onset. Please refer to Fig. 1 for the meaning of each abbreviation.(For interpretation of the references to colour in this figure legend, the reader is referred to the web version of this article.)

to + 1050 ms post-stimulus onset; mixed model coefficient: +0.16%/-trial; 95%CI: +0.08 to + 0.24; uncorrected p-value: 1.701E-04; DF: 1878.00) and in the SFG between + 800 to + 1150 ms post-stimulus onset (maximum t-value: +2.47 noted between + 750 to + 1000 ms post-stimulus onset; mixed model coefficient: +0.06%/-trial; 95%CI: +0.01 to + 0.11; uncorrected p-value: 0.014; DF: 2998.88) (Fig. 4).

The mixed model analysis suggested that increased trial number correlated with persistent reduction of high-gamma amplitude in many brain regions including the frontal, temporal, and parietal lobes (Fig. 4). The largest negative t-value was − 7.34, noted in the precentral gyrus between + 350 to + 600 ms post-stimulus onset (mixed model coefficient: −0.15%/trial; 95%CI: −0.19 to − 0.11; uncorrected p-value:2.536E-13; DF: 5710.02).

3.5. Task familiarity-dependent functional connectivity modulations

Functional connectivity through the frontal aslant fasciculus between the pIFG and SFG was enhanced as a function of trial number, between 700 and 1000 ms post-stimulus onset (Fig. 4**C; Supplementary Video 4**). Of the 736 time windows, 12 (or 1.6%) showed significant positive task familiarity effects on high-gamma amplitudes in mixed model analysis. Thus, there was approximately 3.1% and 0.0008% chance probability of a pair of ROIs showing significant positive effects of task familiarity on high-gamma amplitudes simultaneously for at least one and two consecutive time windows, respectively.

Task familiarity-dependent functional connectivity diminution involved the arcuate, uncinate, superior-longitudinal, inferior-longitudinal, and inferior fronto-occipital fasciculi between the temporal, frontal, parietal, and occipital lobes between the stimulus onset and 500 ms post-stimulus offset (Fig. 4**C; Supplementary Video 4**). Of the 736 time windows, 401 (or 54.5%) showed significant negative effects of task familiarity in the aforementioned mixed model analysis. Thus, there was approximately 24.2%, 7.9%, 2.4% chance probability of two ROIs showing significant negative effects simultaneously for at least five, six, and seven consecutive time windows, respectively.

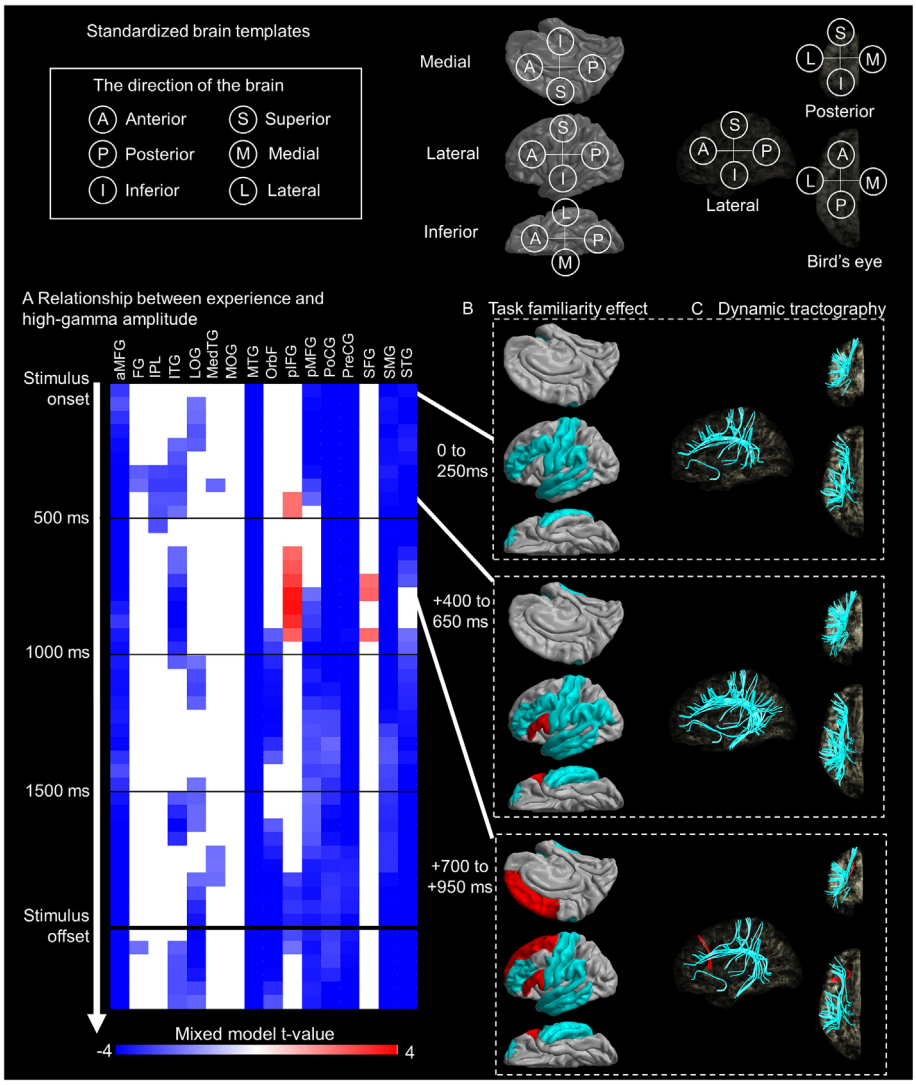

Fig. 4. Task familiarity-dependent high-gamma amplitude modulations and white matter substrates. (A) Spatiotemporal characteristics of the relationship between task familiarity and high-gamma amplitude. The red cells indicate mixed model t-values at regions of interest (ROIs) and corresponding 250-ms time windows where increased trial numbers were significantly associated with increased high-gamma amplitudes. The blue cells indicate time windows where increased trial numbers were significantly associated with decreased high-gamma amplitudes. (B) Snapshots of task familiarity-dependent high-gamma modulations. Color-coded ROIs indicate that increased trial numbers were significantly associated with increased (red) or decreased (blue) high-gamma amplitudes. (C) Snapshots of white matter tracts underlying task familiarity-dependent functional connectivity modulations. Color-coded streamlines indicate functional connectivity enhancement (red) and diminution (blue) between ROIs. 0 ms: a 250-ms time window immediately after stimulus onset. Please refer to Fig. 1 for the meaning of each abbreviation.(For interpretation of the references to colour in this figure legend, the reader is referred to the web version of this article.)

3.6. Covariates associated with task-related high-gamma amplitudes

As ancillary findings from the mixed model analysis, we also observed significant effects of certain other covariates on high-gamma amplitudes. For laterality, the left SFG showed significantly higher high-gamma amplitude compared to the right, between + 600 ms post-stimulus onset to + 500 ms post-stimulus offset, and this effect was particularly large during the response period (maximum t-value: +5.61 noted between + 250 to + 500 ms post-stimulus offset; mixed model coefficient: +7.60% [95%CI: +4.94 to + 10.25]; uncorrected p-value: 2.169E-08; DF: 2770.78).

In addition, high-gamma dynamics varied between trials immediately following a successful versus failed trial. Compared to trials after a successful response, those after a failed response showed attenuated high-gamma amplitudes in the lateral occipital region, between + 100 and + 1,100 ms post-stimulus onset (largest negative t-value: −5.17 noted between + 250 to + 500 ms post-stimulus offset; mixed model coefficient: −8.21% [95%CI: −11.31 to − 5.10]; uncorrected p-value: 2.507E-07; DF: 2172.09; **Supplementary Fig. 1**). In contrast, trials after a failed response were associated with persistent augmentation of high-gamma amplitude in the STG, supramarginal, pMFG, precentral, postcentral, and fusiform regions just after stimulus onset (largest t-value in the fusiform: +8.02 noted between + 50 to + 300 ms post-stimulus offset; mixed model coefficient: 7.17% [95%CI: 5.42 to 8.93]; uncorrected p-value: 1.408E-15; DF: 3586.31; **Supplementary Fig. 1**). For interested readers, **Supplementary Video 5** presents the spatiotemporal dynamics of prior failed response-related high-gamma modulations and functional connectivity.

3.7. Relationship between high-gamma modulations and response accuracy

The logistic mixed model analysis revealed that increased high-gamma amplitude in the pIFG region during two 250-ms periods between stimulus onset and 500-ms post-stimulus onset (Fig. 5)

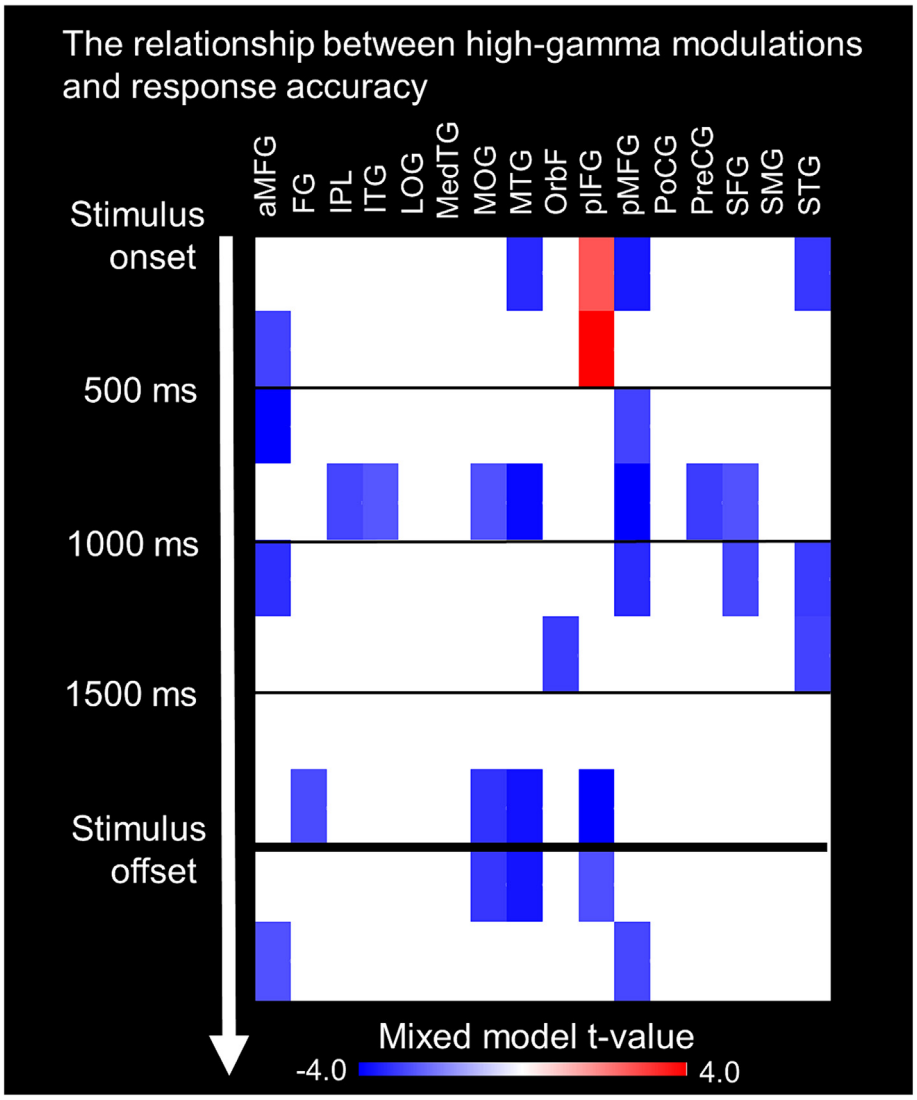

Fig. 5. Relationship between high-gamma modulations and response accuracy. In this matrix of 16 regions of interest (ROIs) and ten 250-ms time windows, the mixed model t-values are shown in the cells, representing the strength of the association between high-gamma amplitude and the likelihood of successful trials. Red cells indicate a significant positive association between high-gamma amplitude and achieving a successful trial. Blue cells indicate a significant negative association, where reduced high-gamma amplitude was associated with a higher chance of successful trials. Please refer to Fig. 1 for the meaning of each abbreviation.(For interpretation of the references to colour in this figure legend, the reader is referred to the web version of this article.)

was associated with a higher chance of the trial being successful, independently of the six covariates. The maximum t-value was + 4.52, observed during the 250-ms period between + 250 to + 500 ms post-stimulus onset; the odds ratio was + 1.01/% (95%CI: +1.005 to + 1.013; uncorrected p-value: 7.180E-06), and the DF was 1880.00.

Additionally, reduced high-gamma amplitude in multiple ROIs in the frontal, temporal, and parietal lobes was independently associated with a higher chance of the trial being successful (Fig. 5). For instance, a decrease in high-gamma amplitude in the aMFG region between + 500 ms and + 750 ms post-stimulus onset was associated with successful trials, with a t-value of − 4.31; thereby, the odds ratio was 0.994/% (95%CI: 0.99 to 1.00; uncorrected p-value: 1.71E-05), and a DF of 2412.00.

The logistic mixed model analysis indicated that an increased memory load was independently associated with a lower chance of a successful trial (Bootstrap mean t-value: –22.95; 95%CI: –23.62 to –22.33; p-value: 9.990E-04). A separate univariate logistic regression analysis revealed that each additional tile decreased the odds of a successful trial by a Bootstrap mean of 0.47 across ten patients (95%CI: 0.35 to 0.59; p-value: 0.002).

3.8. Additive value of high-gamma amplitude in predicting upcoming responses

Based on the machine learning bagged tree ensemble model incorporating a total of 70 variables, the top three predictor variables contributing to accurate prediction of upcoming responses were: [1] 'number of tiles (i.e., memory load)' (Bootstrap mean relative contribution: 0.00288; 95%CI: 0.00285 to 0.00290; p-value: 0.001), [2] 'pIFG high-gamma amplitude between + 250 and + 500 ms post-stimulus onset' (Bootstrap mean relative contribution: 0.000286; 95%CI: 0.000273 to 0.000299; p-value: 0.001), and [3] 'SFG high-gamma amplitude between stimulus onset and 250 ms post-stimulus onset' (Bootstrap mean relative contribution: 0.000249; 95%CI: 0.000236 to 0.000261; p-value: 0.001). It is important to note that the predictive performance of the 'pIFG high-gamma amplitude between + 250 and + 500 ms post-stimulus onset' was significant as evidenced by both logistic mixed model and machine learning-based analyses (see Fig. 5). In contrast, the 'SFG high-gamma amplitude between stimulus onset and 250 ms post-stimulus onset' did not demonstrate significant predictive performance in the logistic mixed model analysis, as shown in Fig. 5.

The base logistic regression model solely incorporating 'the number of tiles in a given trial' predicted a successful trial with an area under the curve (AUC) of 0.72 (95%CI: 0.67 to 0.77). The full logistic regression model, which also incorporated 'pIFG high-gamma amplitude between + 250 and + 500 ms post-stimulus onset' predicted a successful trial with an AUC of 0.76 (95%CI: 0.70 to 0.82). The AUC was improved by 5.74% (95% CI: 3.61 to 7.87) when pIFG high-gamma amplitude was added as a predictor variable, compared to the base logistic regression model without this variable.

3.9. Relationship between task-related high-gamma and other frequency band amplitudes

Fig. 6 depicts snapshots from time-resolved animations showing task-related high-gamma and alpha amplitude modulations.

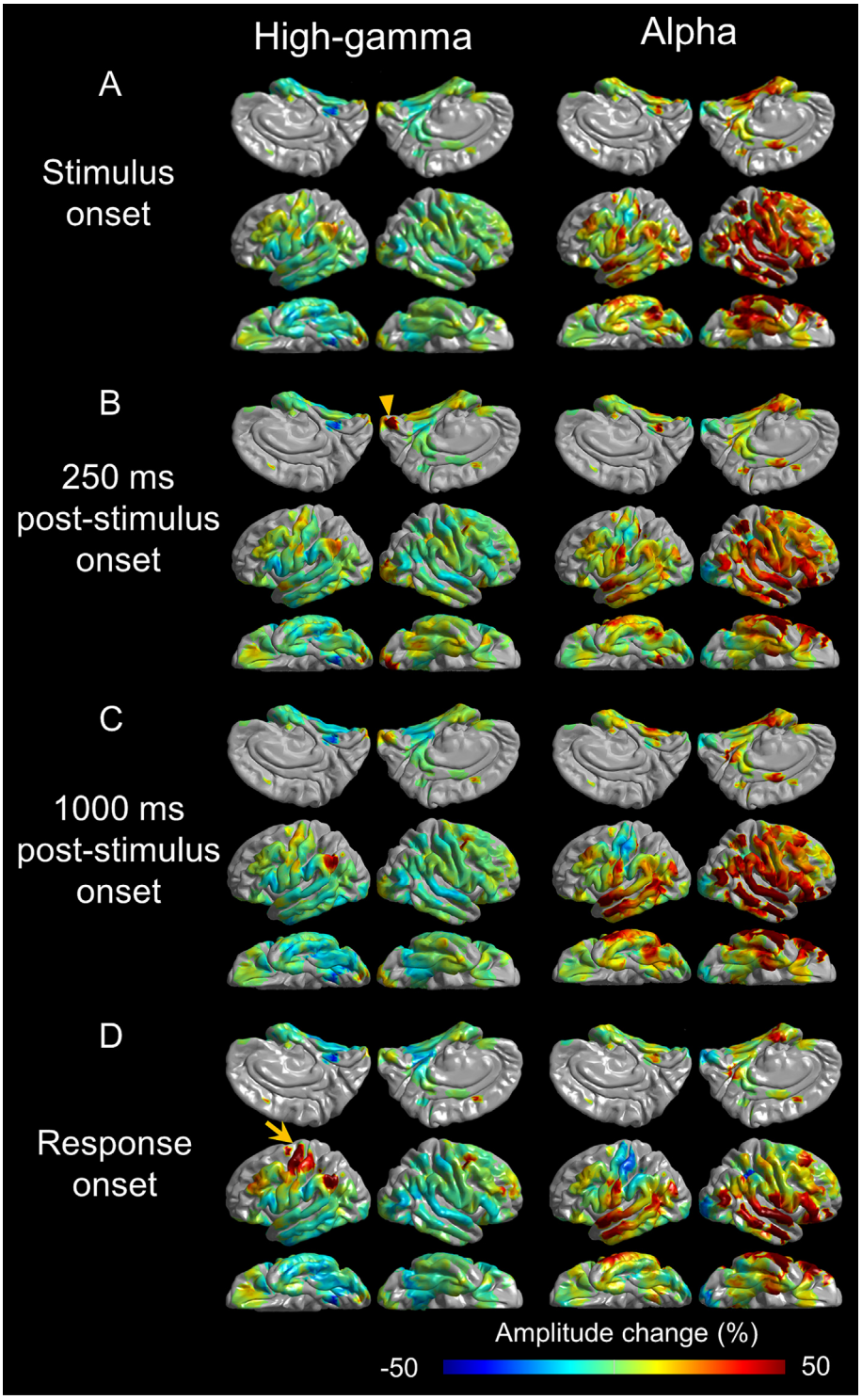

Fig. 6. Task-related high-gamma and alpha amplitude modulations. The snapshots showcase the percent change of high-gamma$_{70\text{-}110\ Hz}$ and alpha$_{8\text{-}12\ Hz}$ amplitudes in comparison to the baseline mean. (A) Stimulus onset. (B) 250 ms after stimulus onset. The arrowhead indicates increased high-gamma amplitude in the right medial occipital region. (C) 1000 ms after stimulus onset. (D) Response onset (i.e., the onset of the first tap response). The arrow indicates increased high-gamma amplitude in the left precentral and postcentral gyri. For a comprehensive overview of the iEEG high-gamma and alpha amplitude changes, please refer to **Supplementary Video 2**.

This visualization reveals increases in high-gamma amplitude, along with reductions in alpha amplitude in the medial occipital region at 250 ms post-stimulus onset (Fig. 6**B**), as well as in the left precentral and postcentral gyri at response onset (Fig. 6**D**). However, after stimulus onset, we observed a persistent and widespread increase in alpha amplitudes, whereas high-gamma amplitudes appeared to be mildly reduced compared to baseline. In Supplementary Figs. 2 - 17, we present the plots showing the temporal changes of task-related high-gamma and other frequency band amplitudes at given ROIs.

Fig. 7 summarizes the correlations between task-related high-gamma and other frequency band amplitudes within specific ROIs. There was an inverse correlation between high-gamma amplitude and each of the low-frequency band amplitudes: delta, theta, alpha, and sigma activities, in a region-specific manner (detailed statistical results in Supplementary Table 2). The degree of inverse correlation between high-gamma and each of the low-frequency band amplitudes was generally modest. The grand-mean Spearman's rho across the 16 ROIs was − 0.08 (95%CI: −0.11 to − 0.05; p-value: 0.004) for delta; −0.08 (95% CI: −0.12 to − 0.05; p-value: 0.001) for theta; −0.08 (95% CI: −0.10 to − 0.06; p-value: 0.001) for alpha; −0.05 (95%CI: −0.09 to − 0.01; p-value: 0.018) for sigma amplitude. Conversely, high-gamma amplitudes were positively correlated with beta, low-gamma, and very high-gamma amplitudes; the grand-mean Spearman's rho across the 16 ROIs was 0.10 (95%CI: 0.03 to 0.16; p-value: 0.019) for beta; 0.29 (95%CI: 0.23 to 0.36; p-value: 0.001) for low-gamma; 0.45 (95%CI: 0.40 to 0.51; p-value: 0.001) for very high-gamma amplitude.

Within the sensorimotor and visual areas, the largest negative rho values were noted when computing the correlation of high-gamma with sigma or alpha amplitude. At the precentral, lateral occipital, and fusiform regions, high-gamma amplitude was most inversely correlated with sigma amplitude (rho: −0.21, −0.11, and − 0.11; p-values: 0.001, 0.042, and 0.016, respectively). At the postcentral gyrus, high-gamma amplitude was most inversely correlated with alpha amplitude (rho: −0.17; p-value: 0.002).

In contrast, within association cortices, the largest negative rho values were noted when computing the correlation of high-gamma with theta or delta amplitude. At the orbitofrontal region, pIFG, STG, and supramarginal gyrus, high-gamma amplitude was most inversely correlated with theta amplitude (rho: −0.14, −0.17, −0.10, and − 0.20; p-values: 0.004, 0.007, 0.015, and 0.001, respectively). At the inferior parietal, inferior temporal, middle-temporal, and anterior middle-frontal gyri, high-gamma amplitude was most inversely correlated with delta amplitude (rho: −0.16, −0.14, −0.10, and − 0.20; p-values: 0.021, 0.007, 0.030 and 0.002).

Given the observed differences in the inverse correlation between high-gamma amplitudes and low-frequency band amplitudes across various ROIs, we conducted a post-hoc mixed model analysis. Detailed methods and results are provided in the **Supplementary document** and **Supplementary Fig. 18**. We found that baseline low-frequency rhythm in the sensorimotor and visual areas, as compared to within the association cortices, was predominantly characterized by relatively higher alpha and sigma amplitudes than theta and delta amplitudes.

Interestingly in the medial temporal region, the mean Spearman's rho between high-gamma and each of the low-frequency

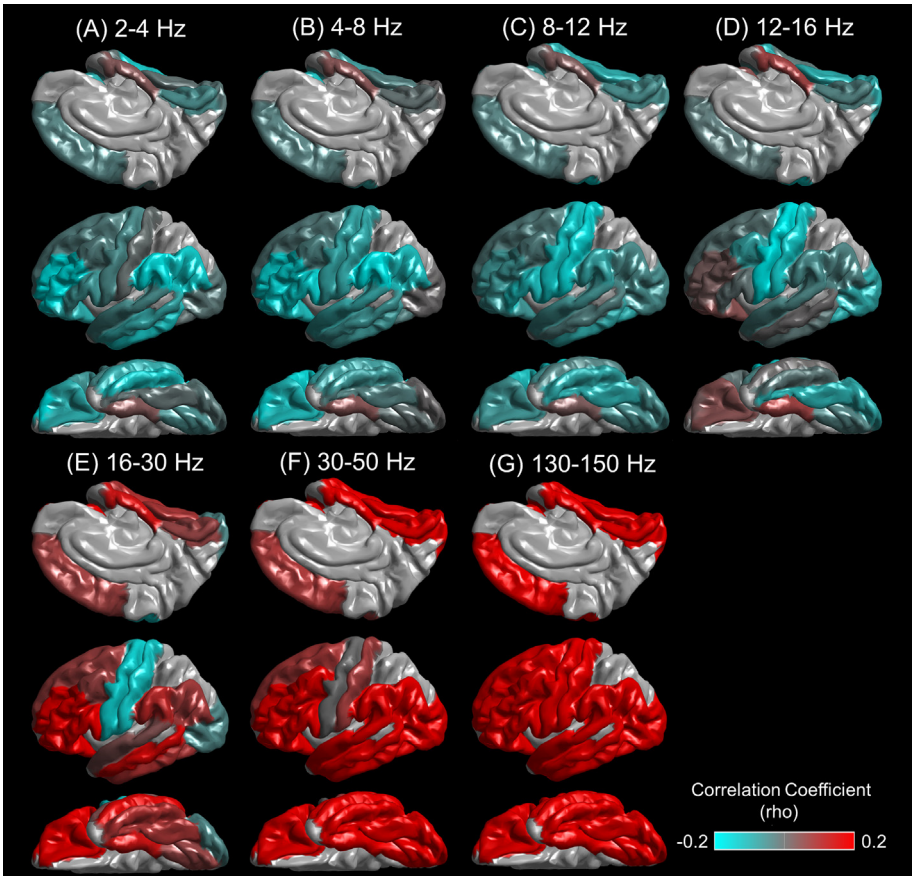

Fig. 7. Correlation between task-related high-gamma and other frequency band amplitudes. The mean Spearman's rho is presented, which reflects the degree of correlation between high-gamma amplitude at 70–110 Hz and one of the following frequency band amplitudes within a given region of interest (ROI). (A) Delta at 2–4 Hz. (B) Theta at 4–8 Hz. (C) Alpha at 8–12 Hz. (D) Sigma at 12–16 Hz. (E) Beta at 16–30 Hz. (F) Low-gamma at 30–50 Hz. (G) Very high-gamma at 130–150 Hz.

band amplitudes did not fall below zero and was relatively higher than those in the remaining 15 ROIs (Fig. 7). For instance, the mean Spearman's rho between high-gamma and alpha amplitudes was + 0.03 within the medial temporal region, higher than the grand mean across the remaining 15 ROIs (grand mean rho across the 15 ROIs: −0.12; 95%CI: −0.14 to − 0.10; p-value: 0.001 on studentized bootstrap one-sample t-test).

4. Discussion

4.1. Summary

We found that the human brain enhances functional connectivity between the occipital and medial temporal regions during stimulus presentation to encode visual information under increased memory load. This is achieved while simultaneously diminishing functional connectivity across other brain regions. Furthermore, we found that with increased familiarity with the task through repeated trials, the pIFG becomes active within the first few hundred milliseconds after stimulus onset, while reducing neural costs across other extensive brain networks. Activation of the pIFG appears to be instrumental in improving working memory function because we observed that increased high-gamma amplitude in the pIFG right after stimulus onset was predictive of successful memory performance. The current study has broadened our understanding of how humans adapt to effectively exert visuospatial working memory function through the modulation of underlying cortical networks via white matter tracts, and our movies illustrate such spatiotemporal dynamics.

4.2. Memory load-dependent functional connectivity enhancement within 1000 ms post-stimulus onset

Our dynamic tractography movies demonstrated enhancement of memory load-dependent functional connectivity through the medial occipital longitudinal tract between the medial occipital region (a lower-order visual area; Nakai et al., 2019) and the medial temporal region between 350 and 800 ms post-stimulus onset (Fig. 3). Early memory load-dependent high-gamma augmentation at the medial occipital region can be attributed to more complex physical properties derived from a larger number of blue-painted tiles or a larger matrix size. Increased complexity or size of visual stimuli may require more saccadic eye movements for successful encoding, and each saccade is expected to transiently augment high-gamma activity in the medial occipital region (Uematsu et al., 2013). Due to the absence of a control task, in which patients would, for example, randomly tap a pre-instructed number of tiles, we are unable to determine the proportion of medial occipital high-gamma augmentation attributable to the physical properties of visual stimuli.

Subsequently, higher-order visual areas, including the fusiform and lateral occipital regions, displayed memory load-dependent high-gamma amplitude enhancement together with the medial occipital and medial temporal regions between 550 and 950 ms post-stimulus onset. The functional connectivity enhancements between the lower-/higher-order visual areas and the medial temporal region may reflect working memory processes, including visual perception, memory encoding, and maintenance. This notion is consistent with a scalp EEG study in healthy individuals that reported successful recall of picture stimuli was associated with increased $gamma_{50\text{-}80\ Hz}$ amplitudes and reduced $alpha_{8\text{-}12\ Hz}$ amplitudes in the posterior head region between 400 to 1,300-ms post-stimulus onset (Friese et al., 2013). Another study of visuospatial working memory in healthy participants using scalp EEG reported that increased number of memory items were associated with increased event-related potentials in the occipital region contralateral to the memorized hemifield during a 900-ms delay/-maintenance period (Vogel and Machizawa, 2004). Lesion-to-deficit studies indicate that the medial temporal lobe structures support accurate visuospatial working memory, based on the observations that patients with bilateral medial temporal lobe damage had profound impairments and even with 4 second delays, these patients could not recall visual stimuli (Olson et al., 2006; Jeneson et al., 2012).

4.3. Memory load-dependent functional connectivity enhancement around stimulus offset

We found a brief memory load-dependent increase in high-gamma amplitude in several regions, including the medial temporal, medial occipital, and pIFG, around the stimulus offset (i.e., around 2000 ms post-stimulus onset; Fig. 3). Functional connectivity enhancement between the medial occipital and pIFG regions took place through the inferior fronto-occipital fasciculus between − 100 and 200 ms post-stimulus offset. Interpretation of this late and brief functional connectivity enhancement is less straightforward. Some hypothesize that it reflects a mediation of attentional control of the visual reactivation process to facilitate optimal retention of memory items. A study of visuospatial memory in nonhuman primates found that the prefrontal region showed increased firing rate based on the visually attended locations, rather than the remembered ones in a task requiring visuospatial working memory function (Lebedev et al., 2004). Furthermore, previous fMRI studies of healthy individuals have reported persistent hemodynamic activation in the dorsolateral prefrontal cortex and the pIFG during a delay/maintenance period of visual working memory tasks (Curtis and D'Esposito, 2003; Rissman et al., 2008).

4.4. Persistent memory load-dependent functional connectivity diminution

We observed memory load-dependent functional connectivity diminution in extensive white matter networks, including the arcuate, uncinate, and superior-longitudinal fasciculi between the temporal, frontal, and parietal lobes, persisting between the stimulus onset and 500 ms post-stimulus offset (Fig. 3). This finding is consistent with the hypothesis of resource reallocation (Mayer et al., 2007; Bays et al., 2011), which suggests that as memory load increases, the brain selectively allocates more attentional and cognitive resources to the relevant regions (i.e., between visual areas and medial temporal region) and reduces connectivity with regions involved in processing irrelevant or distracting information such as environmental sounds. Furthermore, our study found that reduced high-gamma amplitudes in the STG, MTG, precentral gyrus, aMFG, and pMFG (often consisting of a part of the auditory, motor and language networks; (Nakai et al., 2017; Nakai et al., 2019) were associated with higher odds of success (Fig. 5).

4.5. Task familiarity-dependent functional connectivity enhancement involving the posterior inferior frontal gyrus (pIFG)

Our study demonstrated that pIFG high-gamma amplitude was enhanced as a function of trial number, and an increase of early pIFG high-gamma activity during stimulus presentation improved the probability of successful recall. We observed a significant increase in pIFG high-gamma amplitude between + 400 ms and + 900 ms post-stimulus onset with an increased trial number (Fig. 4; **Supplementary Video 4**). Additionally, task familiarity-dependent functional connectivity between pIFG and SFG through

the frontal aslant fasciculus was enhanced between + 800 and 1150 ms post-stimulus onset. Our machine learning-based classification model revealed that pIFG high-gamma amplitude between + 250 to + 500 ms post-stimulus onset had the second largest relative contribution to successful performance, after the number of blue tiles. Namely, the memory load had the largest relative contribution to predict the accuracy of successful recall. Incorporating this pIFG high-gamma measure significantly improved the AUC of the memory load-based logistic regression model in predicting successful trials by 5.74%. Such a small, incremental improvement in memory performance may have a major effect on humans' lives over time or in specific contexts, such as preparing for an exam or a sports match. Our prior iEEG and fMRI studies of children have shown that pIFG is involved in visual memory formation (Ofen et al., 2007; Johnson et al., 2018b; Tang et al., 2018). We hypothesize that early pIFG engagement and functional connectivity enhancement with the SFG through the frontal aslant fasciculus during the stimulus period may reflect attentional control or strategic manipulation of memory items for optimizing visuospatial working memory performance, gained through the experience of more trials (Phillips and Baddeley, 1971; Schmidt et al., 2002; Bunge and Wright, 2007; Eimer, 2014). Functional imaging studies of healthy individuals and invasive neurophysiology studies of non-human primates indicate that the pIFG plays a critical role in selectively attending to relevant visual information to facilitate the encoding and maintenance of the memory items (Coull et al., 1996; Curtis and D'Esposito, 2003; Lebedev et al., 2004; Rissman et al., 2008). Plausible manipulation processes may also include encoding of memory items as chunks or groups of simple forms or motor sequences (Bor et al., 2003; Seidler et al., 2012). Previous fMRI studies of healthy individuals reported bilateral pIFG activation was elicited in visuospatial working memory tasks in which participants were required to exert manipulation, such as chunking of painted tiles in matrices rotated mentally, to judge the identity of two visual stimuli (Mohr et al., 2006; Suchan et al., 2006). A study of healthy individuals reported that repetitive transcranial magnetic stimulation of the SFG, believed to be connected to the pIFG, transiently impaired working memory manipulation function (Postle et al., 2006).

4.6. Persistent task familiarity-dependent functional connectivity diminution

We observed a task familiarity-dependent connectivity diminution in extensive white matter networks, including the arcuate, uncinate, superior-longitudinal, inferior-longitudinal, and inferior fronto-occipital fasciculi between the temporal, frontal, parietal, and occipital lobes. This connectivity diminution persisted during the analysis period between stimulus onset and 500 ms post-stimulus offset (Fig. 4). Our observed task familiarity-dependent connectivity diminution can be attributed to the practice effect or behavioral priming: characterized by a reduction in overall brain processing and also known as repetition suppression (Gotts et al., 2012). Previous iEEG studies have reported task familiarity-dependent reductions in high-gamma amplitude across extensive networks during visual naming, reading, or working memory tasks (McDonald et al., 2010; Merzagora et al., 2014; Vidal et al., 2014; Korzeniewska et al., 2020). Our results generate the hypothesis that engagement of the pIFG would result in a reduction of functional connectivity networks irrelevant to visuospatial working memory. Yet, the current study's data did not provide definitive evidence to support this conjecture, because we observed that the significant decrease in functional connectivity was present from the onset of the stimulus throughout the entirety of the analysis period. Consequently, we were unable to establish a chronological order and definitively determine whether augmentation in pIFG's high-gamma activity precedes this reduction in functional connectivity across widespread brain regions.

4.7. Correlation between high-gamma and low frequency band amplitudes

The Spearman's rho values indicated a modest inverse correlation between high-gamma and multiple low-frequency band amplitudes within all ROIs, except the medial temporal region (Fig. 7 and Supplementary Table 2). Given that event-related high-gamma attenuation indicates cortical deactivation and disengagement (Mukamel et al., 2005; Crone et al., 2006; Nishida et al., 2008; Ray et al., 2008; Harvey et al., 2013; Kunii et al., 2013; Arya et al., 2018; Leszczyński et al., 2020; Hill et al., 2021; Sonoda et al., 2022), the memory load-dependent alpha enhancement, in concert with high-gamma attenuation, observed in this study likely signifies the transient suppression of networks not essential for the working memory task (Jensen and Mazaheri, 2010). Consistently reported findings in both EEG and MEG studies include suppression of posterior alpha amplitude in the hemisphere contralateral to presentation of a remembered stimulus (Mazaheri and Jensen, 2008; Sauseng et al., 2009; van Dijk et al., 2010; Reinhart et al., 2012); such posterior alpha suppression likely reflects underlying cortical excitations to encode visual stimuli. In turn, non-invasive EEG studies have reported that increased working memory loads lead to the enhancement of alpha amplitude in prefrontal and parietal regions (Sauseng et al., 2005; Grimault et al., 2009), which could reflect transient suppression of the underlying cortices.

The current iEEG study demonstrated that, within the sensorimotor and visual areas, high-gamma amplitude was most inversely correlated with amplitude of alpha$_{8\text{-}12\ Hz}$ or sigma activity$_{12\text{-}16\ Hz}$; in contrast, within the association cortices, high-gamma amplitude was most inversely correlated with amplitude of theta$_{4\text{-}8\ Hz}$ or delta activity$_{2\text{-}4\ Hz}$. This observation may help some investigators who want to predict the timing of high-gamma augmentation in a biological model of visuospatial working memory based on the attenuation of low-frequency band activities on scalp EEG or MEG.

Within the medial temporal region, the Spearman's rho between high-gamma and any of the aforementioned low-frequency band amplitudes did not fall below zero, and the rho value was relatively higher than those in the remaining 15 ROIs. This observation suggests that an augmentation of high-gamma activity related to the working memory task does not necessarily co-occur with attenuation of low-frequency band activities in the medial temporal region. In other words, it seems least likely that one could accurately predict the timing of high-gamma augmentation related to working memory tasks solely based on the attenuation of low-frequency band activities in this particular region. A study of adults with focal epilepsy reported that iEEG activity during episodic memory formation differed between the medial temporal and neocortical regions; successful memory was tied to reduced iEEG power at 3–8 Hz in the neocortex and increased power in the medial temporal areas of both hemispheres (Burke et al., 2013).

4.8. Novelty

To the best of our knowledge, this is the first study to present time-resolved animations that visualize millisecond-scale neural modulations at the cortical level and functional connectivity modulations via direct white matter tracts supporting visuospatial working memory. The time-resolved animations were created based on intracranially-recorded high-gamma modulations sampled from 876 nonepileptic sites during a task requiring visuospatial working memory function. We estimated the enhancement of functional connectivity via the white matter tracts by employing the concept that cortical regions showing simultaneous high-

frequency neural responses are likely involved in coordinated interactions (Singer, 1993; Buonomano and Merzenich, 1998; Singer, 2018). Our previous iEEG study found that distant cortical regions showing simultaneous task-related high-gamma augmentation were frequently connected with direct white matter pathways on DWI tractography and accompanied by increased effective connectivity as rated by early neural responses to single-pulse electrical stimulation (Sonoda et al., 2021). Our recent iEEG studies provided video atlases demonstrating the rapid dynamics of white matter functional connectivity modulations during spontaneous eye movements (Ono et al., 2023), picture and auditory naming tasks (Kitazawa et al., 2023), based on the significant and simultaneous high-gamma augmentation beyond a chance level.

The novelty of the present study lies in the segregation and visualization of spatiotemporal dynamics of white matter connectivity modulations that are dependent on 'visuospatial working memory loads' and 'task familiarity'. Specifically, we utilized a mixed model analysis to isolate the unique effects of these factors on high-gamma amplitudes during a working memory task. We employed dynamic tractography imaging technique to visualize biologically plausible direct white matter pathways associated with transient enhancement and diminution of coordinated neural interactions. For instance, the medial occipital longitudinal tract (Beyh et al., 2022) was found to support memory load-dependent functional connectivity enhancement between the medial occipital and medial temporal regions from 350 to 800 ms post-stimulus onset, while the inferior fronto-occipital fasciculus supported the enhanced connectivity between the medial occipital and pIFG around stimulus offset (**Supplementary Video 3**). The frontal aslant fasciculus was involved in task familiarity-dependent connectivity enhancement between the pIFG and SFG between 700 and 1000 ms post-stimulus onset (**Supplementary Video 4**). In contrast, extensive white matter pathways were involved in persistent and extensive diminution of memory load- and task familiarity-dependent functional connectivity (**Supplementary Videos 3 and 4**). We are confident that our video will be a valuable resource for enhancing understanding of the rapid network dynamics underlying visuospatial working memory.

Another novelty of our study lies in the game's adaptive feature where the working memory load in each trial was defined based on the memory performance of a given individual. Drawing a parallel to human experience, as one challenge is met, often the subsequent ones grow in complexity. Because of this adaptive feature, the mean correct response rate effectively ranged around 50% across all study participants. All patients were thus expected to make comparable efforts in the task. Since every participant was given challenging trials and made errors in approximately 50% of those trials, we were able to assess the effect of failed responses in immediately prior trials using mixed model analysis. The mixed model analysis controlling for the memory loads showed that, in trials following a failed response, high-gamma amplitude was attenuated in the lateral and medial occipital regions at 200–450 ms post-stimulus, whereas persistent high-gamma augmentation was noted in the frontal-parietal-temporal regions (**Supplementary** Fig. 1). Such spatiotemporal dynamics of high-gamma modulations related to a prior failed response might be attributed to the notion that, after failed trials, patients may be avoiding automatic or effortless visual processing and exerting error analysis to avoid repeating mistakes (Huster et al., 2011; Rae et al., 2014; Völker et al., 2018; Mitsuhashi et al., 2022).

4.9. Methodological considerations

To the best of our knowledge, no studies have been found that aim to determine the correlation between individual performance in Lumosity Memory Matrix and working memory scales in the Wechsler Intelligence Scale for Children (WISC), such as digit span, picture span, letter-number sequencing, and arithmetic. The stimuli presented during the aforementioned WISC working memory tests include numbers, letters, and pictures of objects that can be named, necessitating linguistic processing for these tasks. An iEEG study of 17 children with drug-resistant focal epilepsy reported that resection of sites showing picture naming-related high-gamma augmentation was associated with a postoperative decline in working memory subscores on WISC (Arya et al., 2019). Conversely, the Memory Matrix employs colored squares as stimuli, indicating it is designed to specifically measure nonverbal visuospatial working memory function. A study involving 2,471 healthy individuals found a correlation between performances in a nonverbal visuospatial working memory task, referred to as Visual Matrix and resembling Lumosity's Memory Matrix, and other working memory tasks, such as listening sentence span ($r^2 = 0.43$) and digit sentence span ($r^2 = 0.43$) (Swanson, 2017). Furthermore, an analysis of 447,665 general users of Lumosity identified a dose–response relationship between sleep duration and improved performance in the Memory Matrix, particularly for sleep durations between 4 to 7 hours (Richards et al., 2017). Clinical data show that Lumosity Memory Matrix may be able to detect neurocognitive impairments in diseased populations. A study of 31 patients with cirrhosis and 28 with pre-cirrhotic chronic liver disease demonstrated that the Memory Matrix discriminated patients with cirrhosis with an area under the curve of 0.77 (Tartaglione et al., 2014).

It is reasonable to hypothesize that older individuals may employ a different strategy from younger ones when performing this working memory task. However, our mixed model analysis did not have sufficient statistical power to detect the effect of development on task-related high-gamma amplitudes, given the participation of only 10 children and substantial variation in the spatial sampling of iEEG signals. To the point, a recent iEEG study, which analyzed 8,251 nonepileptic electrode sites across 114 patients ranging from infancy to adulthood, revealed slightly higher rates of spontaneous high-frequency activity at > 80 Hz in extra-occipital lobe regions in younger children compared to older ones (Sakakura et al., 2023); however, the most pronounced developmental variability in such high-frequency activity occurred during infancy, with minimal changes observed from age nine onwards.

Based on the mixed model analysis, memory load- and task familiarity-dependent diminution of high-gamma amplitudes were identified in substantial proportions of ROIs and analysis time windows. As such, one may wish to consider the risk of Type I error of high-gamma co-attenuation in a pair of ROIs when examining significant functional connectivity modulations. The risk of Type I error was acceptably low in the ROIs where memory load-dependent high-gamma co-attenuation occurred in three consecutive time windows and where task familiarity-dependent high-gamma co-attenuation took place in seven consecutive time windows.

Our dynamic tractography is not designed to estimate the direction of neural propagation during a working memory task. Incorporating the results of Granger-type causality analysis might be beneficial for visualizing the directionality of strengthened connections (Flinker et al., 2015; Giahi Saravani et al., 2019).

It is infeasible to expect that our analytical approach is free from false negative detection of genuine connectivity enhancement between ROIs. Accurately delineating and validating short-range U-fiber streamlines using DWI tractography is challenging due to a known crossing fiber problem and the absence of an optimal gold standard (Movahedian Attar et al., 2020; Wang et al., 2012). This study postulated that cortical sites within the same

gyrus exhibiting memory load-dependent high-gamma enhancement (e.g., the medial occipital gyrus immediately after stimulus onset) could be connected through local white matter pathways.

While white matter development is suggested to be drastic during young childhood and modest during adolescence (Asato et al., 2010; Baum et al., 2022), it's important to emphasize that our study did not aim to identify age-dependent changes in DWI measures or localize aberrant DWI streamlines in specific patients with focal epilepsy. Instead, our goal was to characterize iEEG high gamma-based functional connectivity modulations via major white matter pathways common to the general population. We believe that our study patients and healthy individuals shared similar white matter streamlines for several reasons. In humans, the head size reaches 95% of the adult dimensions by the age of 7 years (Bastir et al., 2006), and the ages of our study patients ranged from 9 to 20 years. Similar to the approach taken by Kitazawa et al. (2023), we excluded patients with massive brain malformations affecting the central, lateral, or calcarine sulcus. Furthermore, we omitted from our analysis any brain regions impacted by epileptiform discharges or structural lesions. Our prior iEEG study (Sonoda et al., 2021) indeed validated a multimodal analysis that combined iEEG measures from non-epileptic cortices of individual patients with open-source DWI data from healthy individuals. In this analysis, we used single-pulse electrical stimulation to measure the latency of neural responses at remote cortical sites and calculated the white matter propagation velocity, defined as the length of a white matter streamline divided by this neural response latency. We thereby computed this propagation velocity using DWI data from both individual patients and healthy individuals, finding a strong correlation (Pearson's r = 0.8) between propagation velocities derived from individual and open-source DWI data.

We evaluated the temporal dynamics of high-gamma modulations using the widely applied Desikan atlas-based ROIs (Desikan et al., 2006; Nakai et al., 2017). Thus, pIFG reported in this study was a summation of pars opercularis (Brodmann area 44) and pars triangularis (Brodmann area 45). Technical difficulties associated with tractography and a limited number of electrode sites for a given ROI prevented us from reducing the size of ROIs further.

Due to the small sample size, our analysis was limited to intrahemispheric connectivity. Likewise, we were unable to determine the effect of sex on iEEG measures. Sampling limitations are inherent in any iEEG study, as all our intracranial electrodes were placed strictly for clinical necessity; we did not expand the iEEG spatial sampling for research purposes (Mercier et al., 2022). Consequently, some ROIs may not have included an ideal number of samples. We anticipate an increase in the amount of stereoelectroencephalography data from deep cortices and thalamic nuclei in the coming decade (Kerezoudis et al., 2022). Future advancements in tractography sensitivity and larger sample sizes through collaboration may enable connectivity analysis across smaller cortical/subcortical ROIs with satisfactory statistical power.

CRediT authorship contribution statement

Riyo Ueda: Conceptualization, Methodology, Formal analysis, Visualization, Writing – original draft. **Kazuki Sakakura:** Methodology, Data curation, Formal analysis, Visualization, Software. **Takumi Mitsuhashi:** Methodology, Visualization, Software. **Masaki Sonoda:** Methodology, Visualization, Software. **Ethan Firestone:** Writing – review & editing. **Naoto Kuroda:** Methodology, Formal analysis. **Yu Kitazawa:** Methodology, Formal analysis. **Hiroshi Uda:** Methodology, Formal analysis. **Aimee F. Luat:** Data acquisition. **Elizabeth L. Johnson:** Conceptualization, Methodology, Writing – review & editing. **Noa Ofen:** Conceptualization, Methodology, Writing – review & editing. **Eishi Asano:** Resources, Supervision, Funding acquisition, Conceptualization, Methodology, Formal analysis, Visualization, Writing – original draft.

Acknowledgments

We are grateful to Sandeep Sood, MD, Neena I. Marupudi, MD, and Jamie MacDougall, RN, BSN, CPN at Children's Hospital of Michigan, for the collaboration and assistance in performing the studies described above. We want to thank Lumos Labs for providing us with the software as a part of the Lumosity Human Cognition Project (https://www.lumosity.com/hcp). This work was supported by the National Institutes of Health (NS064033 to E.A.; MH107512 to N.O.; NS115918 to E.L.J.) and Japan Society for the Promotion of Science (KAKENHI JP23KJ2197 to R.U.; KAKENHI JP22KJ0323 to N.K.).

Appendix A. Supplementary data

Supplementary data to this article can be found online at https://doi.org/10.1016/j.clinph.2024.03.008.

References

Agam Y, Sekuler R. Interactions between working memory and visual perception: An ERP/EEG study. Neuroimage 2007;36:933–42. https://doi.org/10.1016/j.neuroimage.2007.04.014.

Akanuma N, Alarcón G, Lum F, Kissani N, Koutroumanidis M, Adachi N, et al. Lateralising value of neuropsychological protocols for presurgical assessment of temporal lobe epilepsy. Epilepsia 2003;44:408–18. https://doi.org/10.1046/j.1528-1157.2003.24502.x.

AlSkaif T, Dev S, Visser L, Hossari M, van Sark W. A systematic analysis of meteorological variables for PV output power estimation. Renew Energy 2020;153:12–22. https://doi.org/10.1016/j.renene.2020.01.150.

Arya R, Horn PS, Crone NE. ECoG high-gamma modulation versus electrical stimulation for presurgical language mapping. Epilepsy Behav 2018;79:26–33. https://doi.org/10.1016/j.yebeh.2017.10.044.

Arya R, Roth C, Leach JL, Middeler D, Wilson JA, Vannest J, et al. Neuropsychological outcomes after resection of cortical sites with visual naming associated electrocorticographic high-gamma modulation. Epilepsy Res 2019;151:17–23. https://doi.org/10.1016/j.eplepsyres.2019.01.011.

Asano E, Juhász C, Shah A, Sood S, Chugani HT. Role of subdural electrocorticography in prediction of long-term seizure outcome in epilepsy surgery. Brain 2009;132:1038–47. https://doi.org/10.1093/brain/awp025.

Axmacher N, Schmitz DP, Wagner T, Elger CE, Fell J. Interactions between medial temporal lobe, prefrontal cortex, and inferior temporal regions during visual working memory: a combined intracranial EEG and functional magnetic resonance imaging study. J Neurosci 2008;28:7304–12. https://doi.org/10.1523/JNEUROSCI.1778-08.2008.

Baddeley A. Working memory. Science 1992;255:556–9. https://doi.org/10.1126/science.1736359.

Bastir M, Rosas A, O'higgins P. Craniofacial levels and the morphological maturation of the human skull. J Anat 2006;209:637–54. https://doi.org/10.1111/j.1469-7580.2006.00644.x.

Beyh A, Dell'Acqua F, Cancemi D, De Santiago RF, Ffytche D. The medial occipital longitudinal tract supports early stage encoding of visuospatial information. Commun Biol 2022;5:318. https://doi.org/10.1038/s42003-022-03265-4.

Ball K, Smith D, Ellison A, Schenk T. Both egocentric and allocentric cues support spatial priming in visual search. Neuropsychologia 2009;47:1585–91. https://doi.org/10.1016/j.neuropsychologia.2008.11.017.

Bays PM, Gorgoraptis N, Wee N, Marshall L, Husain M. Temporal dynamics of encoding, storage, and reallocation of visual working memory. J Vis 2011;11:1–22. https://doi.org/10.1167/11.10.6.

Bor D, Duncan J, Wiseman RJ, Owen AM. Encoding strategies dissociate prefrontal activity from working memory demand. Neuron 2003;37:361–7. https://doi.org/10.1016/s0896-6273(02)01171-6.

Bowren Jr M, Adolphs R, Bruss J, Manzel K, Corbetta M, Tranel D, et al. Multivariate lesion-behavior mapping of general cognitive ability and its psychometric constituents. J Neurosci 2020;40:8924–37. https://doi.org/10.1523/jneurosci.1415-20.2020.

Bunge SA, Wright SB. Neurodevelopmental changes in working memory and cognitive control. Curr Opin Neurobiol 2007;17:243–50. https://doi.org/10.1016/j.conb.2007.02.005.

Buonomano DV, Merzenich MM. Cortical plasticity: from synapses to maps. Annu Rev Neurosci 1998;21:149–86. https://doi.org/10.1146/annurev.neuro.21.1.149.

Burke JF, Long NM, Zaghloul KA, Sharan AD, Sperling MR, Kahana MJ. Human intracranial high-frequency activity maps episodic memory formation in space and time. Neuroimage 2014;85:834–43. https://doi.org/10.1016/j.neuroimage.2013.06.067.

Burke JF, Zaghloul KA, Jacobs J, Williams RB, Sperling MR, Sharan AD, et al. Synchronous and asynchronous theta and gamma activity during episodic memory formation. J Neurosci 2013;33:292–304. https://doi.org/10.1523/JNEUROSCI.2057-12.2013.

Buzsáki G, Schomburg EW. What does gamma coherence tell us about inter-regional neural communication? Nat Neurosci 2015;18:484–9. https://doi.org/10.1038/nn.3952.

Chase HW, Clark L, Sahakian BJ, Bullmore ET, Robbins TW. Dissociable roles of prefrontal subregions in self-ordered working memory performance. Neuropsychologia 2008;46:2650–61. https://doi.org/10.1016/j.neuropsychologia.2008.04.021.

Christophel TB, Haynes JD. Decoding complex flow-field patterns in visual working memory. Neuroimage 2014;91:43–51. https://doi.org/10.1016/j.neuroimage.2014.01.025.

Constantinidis C, Klingberg T. The neuroscience of working memory capacity and training. Nat Rev Neurosci 2016;17:438–49. https://doi.org/10.1038/nrn.2016.43.

Coull JT, Frith CD, Frackowiak RS, Grasby PM. A fronto-parietal network for rapid visual information processing: a PET study of sustained attention and working memory. Neuropsychologia 1996;34:1085–95. https://doi.org/10.1016/0028-3932(96)00029-2.

Croizé AC, Ragot R, Garnero L, Ducorps A, Pélégrini-Issac M, Dauchot K, et al. Dynamics of parietofrontal networks underlying visuospatial short-term memory encoding. Neuroimage 2004;23:787–99. https://doi.org/10.1016/j.neuroimage.2003.10.052.

Crone EA, Wendelken C, Donohue S, van Leijenhorst L, Bunge SA. Neurocognitive development of the ability to manipulate information in working memory. Proc Natl Acad Sci U S A 2006;103:9315–20. https://doi.org/10.1073/pnas.0510088103.

Curtis CE, D'Esposito M. Persistent activity in the prefrontal cortex during working memory. Trends Cogn Sci 2003;7:415–23. https://doi.org/10.1016/s1364-6613(03)00197-9.

Darki F, Klingberg T. The role of fronto-parietal and fronto-striatal networks in the development of working memory: a longitudinal study. Cereb Cortex 2015;25:1587–95. https://doi.org/10.1093/cercor/bht352.

Davoudi S, Parto Dezfouli M, Knight RT, Daliri MR, Johnson EL. Prefrontal lesions disrupt posterior alpha-gamma coordination of visual working memory representations. J Cogn Neurosci 2021;33:1798–810. https://doi.org/10.1162/jocn_a_01715.

Desikan RS, Ségonne F, Fischl B, Quinn BT, Dickerson BC, Blacker D, et al. An automated labeling system for subdividing the human cerebral cortex on MRI scans into gyral based regions of interest. Neuroimage 2006;31:968–80. https://doi.org/10.1016/j.neuroimage.2006.01.021.

Di X, Biswal BB. Toward task connectomics: examining whole-brain task modulated connectivity in different task domains. Cereb Cortex 2019;29:1572–83. https://doi.org/10.1093/cercor/bhy055.

Edin F, Klingberg T, Johansson P, McNab F, Tegnér J, Compte A. Mechanism for top-down control of working memory capacity. Proc Natl Acad Sci U S A 2009;106:6802–7. https://doi.org/10.1073/pnas.0901894106.

Eimer M. The neural basis of attentional control in visual search. Trends Cogn Sci 2014;18:526–35. https://doi.org/10.1016/j.tics.2014.05.005.

Elton A, Gao W. Task-positive functional connectivity of the default mode network transcends task domain. J Cogn Neurosci 2015;27:2369–81. https://doi.org/10.1162/jocn_a_00859.

Ferreira CT, Vérin M, Pillon B, Levy R, Dubois B, Agid Y. Spatio-temporal working memory and frontal lesions in man. Cortex 1998;34:83–98. https://doi.org/10.1016/s0010-9452(08)70738-x.

Finc K, Bonna K, He X, Lydon-Staley DM, Kühn S, Duch W, et al. Dynamic reconfiguration of functional brain networks during working memory training. Nat Commun 2020;11:2435. https://doi.org/10.1038/s41467-020-15631-z.

Flinker A, Korzeniewska A, Shestyuk AY, Franaszczuk PJ, Dronkers NF, Knight RT, et al. Redefining the role of broca's area in speech. Proc Natl Acad Sci U S A 2015;112:2871–5. https://doi.org/10.1073/pnas.1414491112.

Friese U, Köster M, Hassler U, Martens U, Trujillo-Barreto N, Gruber T. Successful memory encoding is associated with increased cross-frequency coupling between frontal theta and posterior gamma oscillations in human scalp-recorded EEG. Neuroimage 2013;66:642–7. https://doi.org/10.1016/j.neuroimage.2012.11.002.

Galeano Weber EM, Hahn T, Hilger K, Fiebach CJ. Distributed patterns of occipito-parietal functional connectivity predict the precision of visual working memory. Neuroimage 2017;146:404–18. https://doi.org/10.1016/j.neuroimage.2016.10.006.

Ganis G, Schendan HE, Kosslyn SM. Neuroimaging evidence for object model verification theory: Role of prefrontal control in visual object categorization. Neuroimage 2007;34:384–98. https://doi.org/10.1016/j.neuroimage.2006.09.008.

Giahi Saravani A, Forseth KJ, Tandon N, Pitkow X. Dynamic brain interactions during picture naming. ENeuro 2019;6:1–13. https://doi.org/10.1523/ENEURO.0472-18.2019.

Goddard E, Contini EW, Irish M. Exploring information flow from posteromedial cortex during visuospatial working memory: A magnetoencephalography study. J Neurosci 2022;42:5944–55. https://doi.org/10.1523/jneurosci.2129-21.2022.

Gotts SJ, Chow CC, Martin A. Repetition priming and repetition suppression: A case for enhanced efficiency through neural synchronization. Cogn Neurosci 2012;3:227–37. https://doi.org/10.1080/17588928.2012.670617.

Grimault S, Robitaille N, Grova C, Lina JM, Dubarry AS, Jolicoeur P. Oscillatory activity in parietal and dorsolateral prefrontal cortex during retention in visual short-term memory: additive effects of spatial attention and memory load. Hum Brain Mapp 2009;30:3378–92. https://doi.org/10.1002/hbm.20759.

Hanslmayr S, Staresina BP, Bowman H. Oscillations and episodic memory: Addressing the synchronization/ desynchronization conundrum. Trends Neurosci 2016;39:16–25. https://doi.org/10.1016/j.tins.2015.11.004.

Harvey BM, Vansteensel MJ, Ferrier CH, Petridou N, Zuiderbaan W, Aarnoutse EJ, et al. Frequency specific spatial interactions in human electrocorticography: V1 alpha oscillations reflect surround suppression. Neuroimage 2013;65:424–32. https://doi.org/10.1016/j.neuroimage.2012.10.020.

Henderson MM, Rademaker RL, Serences JT. Flexible utilization of spatial- and motor-based codes for the storage of visuo-spatial information. Elife 2022;11. e75688. https://doi.org/10.7554/eLife.75688.

Hill PF, Seger SE, Yoo HB, King DR, Wang DX, Lega BC, et al. Distinct neurophysiological correlates of the fMRI BOLD signal in the hippocampus and neocortex. J Neurosci 2021;41:6343–52. https://doi.org/10.1523/jneurosci.0278-21.2021.

Hillary FG, Genova HM, Chiaravalloti ND, Rypma B, DeLuca J. Prefrontal modulation of working memory performance in brain injury and disease. Hum Brain Mapp 2006;27:837–47. https://doi.org/10.1002/hbm.20226.

Hoechstetter K, Bornfleth H, Weckesser D, Ille N, Berg P, Scherg M. BESA source coherence: a new method to study cortical oscillatory coupling. Brain Topogr 2004;16:233–8. https://doi.org/10.1023/b:brat.0000032857.55223.5d.

Huster RJ, Eichele T, Enriquez-Geppert S, Wollbrin A, Kugel H, Konrad C, et al. Multimodal imaging of functional networks and event-related potentials in performance monitoring. Neuroimage 2011;56:1588–97. https://doi.org/10.1016/j.neuroimage.2011.03.039.

Jeneson A, Wixted JT, Hopkins RO, Squire LR. Visual working memory capacity and the medial temporal lobe. J Neurosci 2012;32:3584–9. https://doi.org/10.1523/jneurosci.6444-11.2012.

Jensen O, Mazaheri A. Shaping functional architecture by oscillatory alpha activity: gating by inhibition. Front Hum Neurosci 2010;4:186. https://doi.org/10.3389/fnhum.2010.00186.

Johnson EL, Adams JN, Solbakk AK, Endestad T, Larsson PG, Ivanovic J, et al. Dynamic frontotemporal systems process space and time in working memory. PLoS Biol 2018a;16. e2004274. https://doi.org/10.1371/journal.pbio.2004274.

Johnson EL, Dewar CD, Solbakk AK, Endestad T, Meling TR, Knight RT. Bidirectional frontoparietal oscillatory systems support working memory. Curr Biol 2017;27:1829–1835.e4. https://doi.org/10.1016/j.cub.2017.05.046.

Johnson EL, Kam JWY, Tzovara A, Knight RT. Insights into human cognition from intracranial EEG: A review of audition, memory, internal cognition, and causality. J Neural Eng 2020;17. 051001. https://doi.org/10.1088/1741-2552/abb7a5.

Johnson EL, Knight RT. How Can iEEG Be Used to Study Inter-Individual and Developmental Differences? In: Nikolai A Editor., Intracranial EEG: A Guide for Cognitive Neuroscientists. New York: Springer International Publishing; 2023. Pp. 143-154.

Johnson EL, Tang L, Yin Q, Asano E, Ofen N. Direct brain recordings reveal prefrontal cortex dynamics of memory development. Sci Adv 2018b;4. eaat3702. https://doi.org/10.1126/sciadv.aat3702.

Johnson EL, Yin Q, O'Hara NB, Tang L, Jeong JW, Asano E, et al. Dissociable oscillatory theta signatures of memory formation in the developing brain. Curr Biol 2022;32:1457–1469.e4. https://doi.org/10.1016/j.cub.2022.01.053.

Kas A, de Souza LC, Samri D, Bartolomeo P, Lacomblez L, Kalafat M, et al. Neural correlates of cognitive impairment in posterior cortical atrophy. Brain 2011;134:1464–78. https://doi.org/10.1093/brain/awr055.

Kerezoudis P, Gyftopoulos A, Alexander AY, Keith Starnes D, Nickels KC, Worrell GA, et al. Safety and efficacy of responsive neurostimulation in the pediatric population: Evidence from institutional review and patient-level meta-analysis. Epilepsy Behav 2022;129. 108646. https://doi.org/10.1016/j.yebeh.2022.108646.

Kitazawa Y, Sonoda M, Sakakura K, Mitsuhashi T, Firestone E, Ueda R, et al. Intra- and inter-hemispheric network dynamics supporting object recognition and speech production. Neuroimage 2023;270. 119954. https://doi.org/10.1016/j.neuroimage.2023.119954.

Korzeniewska A, Wang Y, Benz HL, Fifer MS, Collard M, Milsap G, et al. Changes in human brain dynamics during behavioral priming and repetition suppression. Prog Neurobiol 2020;189. 101788. https://doi.org/10.1016/j.pneurobio.2020.101788.

Krasnow B, Tamm L, Greicius MD, Yang T, Glover GH, Reiss AL, et al. Comparison of fMRI activation at 3 and 1.5 T during perceptual, cognitive, and affective processing. Neuroimage 2003;18:813–26. https://doi.org/10.1016/s1053-8119(03)00002-8.

Kundu B, Sutterer DW, Emrich SM, Postle BR. Strengthened effective connectivity underlies transfer of working memory training to tests of short-term memory and attention. J Neurosci 2013;33:8705–15. https://doi.org/10.1523/jneurosci.5565-12.2013.

Kunii N, Kamada K, Ota T, Kawai K, Saito N. Characteristic profiles of high gamma activity and blood oxygenation level-dependent responses in various language areas. Neuroimage 2013;65:242–9. https://doi.org/10.1016/j.neuroimage.2012.09.059.

Kural MA, Duez L, Sejer Hansen V, Larsson PG, Rampp S, Schulz R, et al. Criteria for defining interictal epileptiform discharges in EEG: A clinical validation study. Neurology 2020;94:e2139–47. https://doi.org/10.1212/wnl.0000000000009439.

Kuroda N, Sonoda M, Miyakoshi M, Nariai H, Jeong JW, Motoi H, et al. Objective interictal electrophysiology biomarkers optimize prediction of epilepsy surgery outcome. Brain Commun 2021;3. fcab042. https://doi.org/10.1093/braincomms/fcab042.
Kwon H, Reiss AL, Menon V. Neural basis of protracted developmental changes in visuo-spatial working memory. Proc Natl Acad Sci U S A 2002;99:13336–41. https://doi.org/10.1073/pnas.162486399.
LaBar KS, Gitelman DR, Parrish TB, Mesulam M. Neuroanatomic overlap of working memory and spatial attention networks: a functional MRI comparison within subjects. Neuroimage 1999;10:695–704. https://doi.org/10.1006/nimg.1999.0503.
Lebedev MA, Messinger A, Kralik JD, Wise SP. Representation of attended versus remembered locations in prefrontal cortex. PLoS Biol 2004;2:e365. https://doi.org/10.1371/journal.pbio.0020365.
Swanson HL. Verbal and visual-spatial working memory: What develops over a life span? Dev Psychol 2017;53:971–95. https://doi.org/10.1037/dev0000291.
Leszczyński M, Barczak A, Kajikawa Y, Ulbert I, Falchier AY, Tal I, et al. Dissociation of broadband high-frequency activity and neuronal firing in the neocortex. Sci Adv 2020;6. eabb0977. https://doi.org/10.1126/sciadv.abb0977.
Lozano-Soldevilla D, ter Huurne N, Cools R, Jensen O. GABAergic modulation of visual gamma and alpha oscillations and its consequences for working memory performance. Curr Biol 2014;24:2878–87. https://doi.org/10.1016/j.cub.2014.10.017.
Lugtmeijer S, Geerligs L, Tsvetanov KA, Mitchell DJ, Cam-Can, Campbell KL. Lifespan differences in visual short-term memory load-modulated functional connectivity. Neuroimage 2023;270. 119982. https://doi.org/10.1016/j.neuroimage.2023.119982.
Ma WJ, Husain M, Bays PM. Changing concepts of working memory. Nat Neurosci 2014;17:347–56. https://doi.org/10.1038/nn.3655.
Mankin EA, Aghajan ZM, Schuette P, Tran ME, Tchemodanov N, Titiz A, et al. Stimulation of the right entorhinal white matter enhances visual memory encoding in humans. Brain stimul 2021;14:131–40. https://doi.org/10.1016/j.brs.2020.11.015.
Mayer JS, Bittner RA, Nikolić D, Bledowski C, Goebel R, Linden DE. Common neural substrates for visual working memory and attention. Neuroimage 2007;36:441–53. https://doi.org/10.1016/j.neuroimage.2007.03.007.
Mazaheri A, Jensen O. Asymmetric amplitude modulations of brain oscillations generate slow evoked responses. J Neurosci 2008;28:7781–7. https://doi.org/10.1523/jneurosci.1631-08.2008.
McDonald CR, Thesen T, Carlson C, Blumberg M, Girard HM, Trongnetrpunya A, et al. Multimodal imaging of repetition priming: using fMRI, MEG, and intracranial EEG to reveal spatiotemporal profiles of word processing. Neuroimage 2010;53:707–17. https://doi.org/10.1016/j.neuroimage.2010.06.069.
Mercier MR, Dubarry AS, Tadel F, Avanzini P, Axmacher N, Cellier D, et al. Advances in human intracranial electroencephalography research, guidelines and good practices. Neuroimage 2022;260. 119438. https://doi.org/10.1016/j.neuroimage.2022.119438.
Merzagora AR, Coffey TJ, Sperling MR, Sharan A, Litt B, Baltuch G, et al. Repeated stimuli elicit diminished high-gamma electrocorticographic responses. Neuroimage 2014;85:844–52. https://doi.org/10.1016/j.neuroimage.2013.07.006.
Michels L, Bucher K, Lüchinger R, Klaver P, Martin E, Jeanmonod D, et al. Simultaneous EEG-fMRI during a working memory task: modulations in low and high frequency bands. PLoS One 2010;5. e10298. https://doi.org/10.1371/journal.pone.0010298.
Miotto EC, Savage CR, Evans JJ, Wilson BA, Martins MG, Iaki S, et al. Bilateral activation of the prefrontal cortex after strategic semantic cognitive training. Hum Brain Mapp 2006;27:288–95. https://doi.org/10.1002/hbm.20184.
Mitsuhashi T, Sonoda M, Firestone E, Sakakura K, Jeong JW, Luat AF, et al. Temporally and functionally distinct large-scale brain network dynamics supporting task switching. Neuroimage 2022;254. 119126. https://doi.org/10.1016/j.neuroimage.2022.119126.
Mitsuhashi T, Sonoda M, Sakakura K, Jeong JW, Luat AF, Sood S, et al. Dynamic tractography-based localization of spike sources and animation of spike propagations. Epilepsia 2021;62:2372–84. https://doi.org/10.1111/epi.17025.
Möddel G, Lineweaver T, Schuele SU, Reinholz J, Loddenkemper T. Atypical language lateralization in epilepsy patients. Epilepsia 2009;50:1505–16. https://doi.org/10.1111/j.1528-1167.2008.02000.x.
Mohr HM, Goebel R, Linden DE. Content- and task-specific dissociations of frontal activity during maintenance and manipulation in visual working memory. J Neurosci 2006;26:4465–71. https://doi.org/10.1523/jneurosci.5232-05.2006.
Movahedian Attar F, Kirilina E, Haenelt D, Pine KJ, Trampel R, Edwards LJ, Weiskopf N. Mapping short association fibers in the early cortical visual processing stream using in vivo diffusion tractography. Cereb Cortex 2020;30:4496–514. https://doi.org/10.1093/cercor/bhaa049.
Mukamel R, Gelbard H, Arieli A, Hasson U, Fried I, Malach R. Coupling between neuronal firing, field potentials, and FMRI in human auditory cortex. Science 2005;309:951–4. https://doi.org/10.1126/science.1110913.
Nakai Y, Jeong JW, Brown EC, Rothermel R, Kojima K, Kambara T, et al. Three- and four-dimensional mapping of speech and language in patients with epilepsy. Brain 2017;140:1351–70. https://doi.org/10.1093/brain/awx051.
Nakai Y, Sugiura A, Brown EC, Sonoda M, Jeong JW, Rothermel R, et al. Four-dimensional functional cortical maps of visual and auditory language: Intracranial recording. Epilepsia 2019;60:255–67. https://doi.org/10.1111/epi.14648.
Nir Y, Fisch L, Mukamel R, Gelbard-Sagiv H, Arieli A, Fried I, et al. Coupling between neuronal firing rate, gamma LFP, and BOLD fMRI is related to interneuronal correlations. Curr Biol 2007;17:1275–85. https://doi.org/10.1016/j.cub.2007.06.066.
Nishida M, Juhász C, Sood S, Chugani HT, Asano E. Cortical glucose metabolism positively correlates with gamma-oscillations in nonlesional focal epilepsy. Neuroimage 2008;42:1275–84. https://doi.org/10.1016/j.neuroimage.2008.06.027.
O'Connell MA, Basak C. Effects of task complexity and age-differences on task-related functional connectivity of attentional networks. Neuropsychologia 2018;114:50–64. https://doi.org/10.1016/j.neuropsychologia.2018.04.013.
Ofen N, Kao YC, Sokol-Hessner P, Kim H, Whitfield-Gabrieli S, Gabrieli JD. Development of the declarative memory system in the human brain. Nat neurosci 2007;10:1198–205. https://doi.org/10.1038/nn1950.
Olson IR, Moore KS, Stark M, Chatterjee A. Visual working memory is impaired when the medial temporal lobe is damaged. J Cogn Neurosci 2006;18:1087–97. https://doi.org/10.1162/jocn.2006.18.7.1087.
Ono H, Sonoda M, Sakakura K, Kitazawa Y, Mitsuhashi T, Firestone E, et al. Dynamic cortical and tractography atlases of proactive and reactive alpha and high-gamma activities. Brain Commun 2023;5. fcad111. https://doi.org/10.1093/braincomms/fcad111.
Papp N, Ktonas P. Critical evaluation of complex demodulation techniques for the quantification of bioelectrical activity. Biomed Sci Instrum 1977;13:135–45.
Parto Dezfouli M, Davoudi S, Knight RT, Daliri MR, Johnson EL. Prefrontal lesions disrupt oscillatory signatures of spatiotemporal integration in working memory. Cortex 2021;138:113–26. https://doi.org/10.1016/j.cortex.2021.01.016.
Pavlov YG, Kotchoubey B. Oscillatory brain activity and maintenance of verbal and visual working memory: A systematic review. Psychophysiology 2022;59. e13735. https://doi.org/10.1111/psyp.13735.
Peylo C, Friedrich EVC, Minarik T, Biel AL, Sauseng P. Theta:gamma phase coupling and evoked gamma activity reflect the fidelity of mental templates during memory matching in visual perception. Cereb Cortex 2022;32:4156–71. https://doi.org/10.1093/cercor/bhab472.
Phillips W, Baddeley A. Reaction time and short-term visual memory. Psychol Sci 1971;22:73–4. https://doi.org/10.3758/BF03332500.
Pisella L, Alahyane N, Blangero A, Thery F, Blanc S, Pelisson D. Right-hemispheric dominance for visual remapping in humans. Philos Trans R Soc Lond B Biol Sci 2011;366:572–85. https://doi.org/10.1098/rstb.2010.0258.
Pochon JB, Levy R, Poline JB, Crozier S, Lehéricy S, Pillon B, et al. The role of dorsolateral prefrontal cortex in the preparation of forthcoming actions: an fMRI study. Cereb Cortex 2001;11:260–6. https://doi.org/10.1093/cercor/11.3.260.
Postle BR, Ferrarelli F, Hamidi M, Feredoes E, Massimini M, Peterson M, et al. Repetitive transcranial magnetic stimulation dissociates working memory manipulation from retention functions in the prefrontal, but not posterior parietal, cortex. J Cogn Neurosci 2006;18:1712–22. https://doi.org/10.1162/jocn.2006.18.10.1712.
Proskovec AL, Wiesman AI, Heinrichs-Graham E, Wilson TW. Beta oscillatory dynamics in the prefrontal and superior temporal cortices predict spatial working memory performance. Sci Rep 2018;8:8488. https://doi.org/10.1038/s41598-018-26863-x.
Rae CL, Hughes LE, Weaver C, Anderson MC, Rowe JB. Selection and stopping in voluntary action: a meta-analysis and combined fMRI study. Neuroimage 2014;86:381–91. https://doi.org/10.1016/j.neuroimage.2013.10.012.
Rasmussen T, Milner B. The role of early left-brain injury in determining lateralization of cerebral speech functions. Ann N Y Acad Sci 1977;299:355–69. https://doi.org/10.1111/j.1749-6632.1977.tb41921.x.
Ray S, Crone NE, Niebur E, Franaszczuk PJ, Hsiao SS. Neural correlates of high-gamma oscillations (60–200 Hz) in macaque local field potentials and their potential implications in electrocorticography. J Neurosci 2008;28:11526–36. https://doi.org/10.1523/jneurosci.2848-08.2008.
Reinhart RM, Heitz RP, Purcell BA, Weigand PK, Schall JD, Woodman GF. Homologous mechanisms of visuospatial working memory maintenance in macaque and human: properties and sources. J Neurosci 2012;32:7711–22. https://doi.org/10.1523/JNEUROSCI.0215-12.2012.
Reinhart RMG, Nguyen JA. Working memory revived in older adults by synchronizing rhythmic brain circuits. Nat Neurosci 2019;22:820–7. https://doi.org/10.1038/s41593-019-0371-x.
Richards A, Inslicht SS, Metzler TJ, Mohlenhoff BS, Rao MN, O'Donovan A, et al. Sleep and cognitive performance from teens to old age: more is not better. Sleep 2017;40. zsw029. https://doi.org/10.1093/sleep/zsw029.
Rich EL, Wallis JD. Spatiotemporal dynamics of information encoding revealed in orbitofrontal high-gamma. Nat Commun 2017;8:1139. https://doi.org/10.1038/s41467-017-01253-5.
Rissman J, Gazzaley A, D'Esposito M. Dynamic adjustments in prefrontal, hippocampal, and inferior temporal interactions with increasing visual working memory load. Cereb Cortex 2008;18:1618–29. https://doi.org/10.1093/cercor/bhm195.
Roux F, Wibral M, Mohr HM, Singer W, Uhlhaas PJ. Gamma-band activity in human prefrontal cortex codes for the number of relevant items maintained in working memory. J Neurosci 2012;32:12411–20. https://doi.org/10.1523/jneurosci.0421-12.2012.
Sakakura K, Sonoda M, Mitsuhashi T, Kuroda N, Firestone E, O'Hara N, et al. Developmental organization of neural dynamics supporting auditory

perception. Neuroimage 2022;258. 119342. https://doi.org/10.1016/j.neuroimage.2022.119342.
Sakakura K, Kuroda N, Sonoda M, Mitsuhashi T, Firestone E, Luat AF, et al. Developmental atlas of phase-amplitude coupling between physiologic high-frequency oscillations and slow waves. Nat Commun 2023;14:6435. https://doi.org/10.1038/s41467-023-42091-y.
Sato J, Mossad SI, Wong SM, Hunt BAE, Dunkley BT, Smith ML, et al. Alpha keeps it together: Alpha oscillatory synchrony underlies working memory maintenance in young children. Dev Cogn Neurosci 2018;34:114–23. https://doi.org/10.1016/j.dcn.2018.09.001.
Sauseng P, Klimesch W, Doppelmayr M, Pecherstorfer T, Freunberger R, Hanslmayr S. EEG alpha synchronization and functional coupling during top-down processing in a working memory task. Hum Brain Mapp 2005;26:148–55. https://doi.org/10.1002/hbm.20150.
Sauseng P, Klimesch W, Heise KF, Gruber WR, Holz E, Karim AA. Brain oscillatory substrates of visual short-term memory capacity. Curr Biol 2009;19:1846–52. https://doi.org/10.1016/j.cub.2009.08.062.
Schmidt BK, Vogel EK, Woodman GF, Luck SJ. Voluntary and automatic attentional control of visual working memory. Percept Psychophys 2002;64:754–63. https://doi.org/10.3758/bf03194742.
Schmidt D, Krause BJ, Weiss PH, Fink GR, Shah NJ, Amorim MA, et al. Visuospatial working memory and changes of the point of view in 3D space. Neuroimage 2007;36:955–68. https://doi.org/10.1016/j.neuroimage.2007.03.050.
Schmidt TT, Blankenburg F. Brain regions that retain the spatial layout of tactile stimuli during working memory–A 'tactospatial sketchpad'? Neuroimage 2018;178:531–9. https://doi.org/10.1016/j.neuroimage.2018.05.076.
Schneiders JA, Opitz B, Krick CM, Mecklinger A. Separating intra-modal and across-modal training effects in visual working memory: an fMRI investigation. Cereb Cortex 2011;21:2555–64. https://doi.org/10.1093/cercor/bhr037.
Seidler RD, Bo J, Anguera JA. Neurocognitive contributions to motor skill learning: the role of working memory. J Mot Behav 2012;44:445–53. https://doi.org/10.1080/00222895.2012.672348.
Shine JM, Koyejo O, Bell PT, Gorgolewski KJ, Gilat M, Poldrack RA. Estimation of dynamic functional connectivity using multiplication of temporal derivatives. Neuroimage 2015;122:399–407. https://doi.org/10.1016/j.neuroimage.2015.07.064.
Singer W. Synchronization of cortical activity and its putative role in information processing and learning. Annu Rev Physiol 1993;55:349–74. https://doi.org/10.1146/annurev.ph.55.030193.002025.
Singer W. The role of oscillations and synchrony in the development of the nervous system. In: Benasich AA, Ribary U, Lupp J, editors. Emergent Brain Dynamics. Prebirth to Adolescence. Strüngmann Forum Reports. Massachusetts: MIT Press; 2018. p.15-32. https://hdl.handle.net/21.11116/0000-000D-151C-D.
Smith EE, Jonides J. Storage and executive processes in the frontal lobes. Science 1999;283:1657–61. https://doi.org/10.1126/science.283.5408.1657.
Sonoda M, Rothermel R, Carlson A, Jeong JW, Lee MH, Hayashi T, et al. Naming-related spectral responses predict neuropsychological outcome after epilepsy surgery. Brain 2022;145:517–30. https://doi.org/10.1093/brain/awab318.
Sonoda M, Silverstein BH, Jeong JW, Sugiura A, Nakai Y, Mitsuhashi T, et al. Six-dimensional dynamic tractography atlas of language connectivity in the developing brain. Brain 2021;144:3340–54. https://doi.org/10.1093/brain/awab225.
Srimal R, Curtis CE. Persistent neural activity during the maintenance of spatial position in working memory. Neuroimage 2008;39:455–68. https://doi.org/10.1016/j.neuroimage.2007.08.040.
Stolk A, Griffin S, van der Meij R, Dewar C, Saez I, Lin JJ, et al. Integrated analysis of anatomical and electrophysiological human intracranial data. Nat Protoc 2018;13:1699–723. https://doi.org/10.1038/s41596-018-0009-6.
Suchan B, Botko R, Gizewski E, Forsting M, Daum I. Neural substrates of manipulation in visuospatial working memory. Neuroscience 2006;139:351–7. https://doi.org/10.1016/j.neuroscience.2005.08.020.
Suthana NA, Parikshak NN, Ekstrom AD, Ison MJ, Knowlton BJ, Bookheimer SY, et al. Specific responses of human hippocampal neurons are associated with better memory. Proc Natl Acad Sci U S A 2015;112:10503–8. https://doi.org/10.1073/pnas.1423036112.
Tang L, Shafer AT, Ofen N. Prefrontal cortex contributions to the development of memory formation. Cereb Cortex 2018;28:3295–308. https://doi.org/10.1093/cercor/bhx200.
Tartaglione EV, Derleth M, Yu L, Ioannou GN. Can computerized brain training games be used to identify early cognitive impairment in cirrhosis? Am J Gastroenterol 2014;109:316–23. https://doi.org/10.1038/ajg.2013.306.
Toepper M, Markowitsch HJ, Gebhardt H, Beblo T, Bauer E, Woermann FG, et al. The impact of age on prefrontal cortex integrity during spatial working memory retrieval. Neuropsychologia 2014;59:157–68. https://doi.org/10.1016/j.neuropsychologia.2014.04.020.
Thompson TW, Waskom ML, Gabrieli JD. Intensive working memory training produces functional changes in large-scale frontoparietal networks. J Cogn Neurosci 2016;28:575–88. https://doi.org/10.1162/jocn_a_00916.
Uematsu M, Matsuzaki N, Brown EC, Kojima K, Asano E. Human occipital cortices differentially exert saccadic suppression: Intracranial recording in children. Neuroimage 2013;83:224–36. https://doi.org/10.1016/j.neuroimage.2013.06.046.
van Dijk H, van der Werf J, Mazaheri A, Medendorp WP, Jensen O. Modulations in oscillatory activity with amplitude asymmetry can produce cognitively relevant event-related responses. Proc Natl Acad Sci U S A 2010;107:900–5. https://doi.org/10.1073/pnas.0908821107.
Vetter P, Smith FW, Muckli L. Decoding sound and imagery content in early visual cortex. Curr Biol 2014;24:1256–62. https://doi.org/10.1016/j.cub.2014.04.020.
Vidal JR, Perrone-Bertolotti M, Levy J, De Palma L, Minotti L, Kahane P, et al. Neural repetition suppression in ventral occipito-temporal cortex occurs during conscious and unconscious processing of frequent stimuli. Neuroimage 2014;95:129–35. https://doi.org/10.1016/j.neuroimage.2014.03.049.
Vogel EK, Machizawa MG. Neural activity predicts individual differences in visual working memory capacity. Nature 2004;428:748–51. https://doi.org/10.1038/nature02447.
Völker M, Fiederer LDJ, Berberich S, Hammer J, Behncke J, Kršek P, et al. The dynamics of error processing in the human brain as reflected by high-gamma activity in noninvasive and intracranial EEG. Neuroimage 2018;173:564–79. https://doi.org/10.1016/j.neuroimage.2018.01.059.
Vuontela V, Steenari MR, Carlson S, Koivisto J, Fjällberg M, Aronen ET. Audiospatial and visuospatial working memory in 6–13 year old school children. Learn Mem 2003;10:74–81. https://doi.org/10.1101/lm.53503.
Wang C, Xu T, Geng F, Hu Y, Wang Y, Liu H, et al. Training on abacus-based mental calculation enhances visuospatial working memory in children. J Neurosci 2019;39:6439–48. https://doi.org/10.1523/jneurosci.3195-18.2019.
Wang JY, Abdi H, Bakhadirov K, Diaz-Arrastia R, Devous MD. A comprehensive reliability assessment of quantitative diffusion tensor tractography. Neuroimage 2012;60:1127–38. https://doi.org/10.1016/j.neuroimage.2011.12.062.
Wu Z, Buckley MJ. Prefrontal and medial temporal lobe cortical contributions to visual short-term memory. J Cogn Neurosci 2022;35:27–43. https://doi.org/10.1162/jocn_a_01937.
Yaple ZA, Stevens WD, Arsalidou M. Meta-analyses of the n-back working memory task: fMRI evidence of age-related changes in prefrontal cortex involvement across the adult lifespan. Neuroimage 2019;196:16–31. https://doi.org/10.1016/j.neuroimage.2019.03.074.
Yeh FC, Panesar S, Fernandes D, Meola A, Yoshino M, Fernandez-Miranda JC, et al. Population-averaged atlas of the macroscale human structural connectome and its network topology. Neuroimage 2018;178:57–68. https://doi.org/10.1016/j.neuroimage.2018.05.027.
Yin Q, Johnson EL, Tang L, Auguste KI, Knight RT, Asano E, et al. Direct brain recordings reveal occipital cortex involvement in memory development. Neuropsychologia 2020;148. 107625. https://doi.org/10.1016/j.neuropsychologia.2020.107625.
Zumer JM, Scheeringa R, Schoffelen JM, Norris DG, Jensen O. Occipital alpha activity during stimulus processing gates the information flow to object-selective cortex. PLoS Biol 2014;12. e1001965. https://doi.org/10.1371/journal.pbio.1001965.